

2

AD-A233 574

CRACK GROWTH PROCESSES AT ELEVATED TEMPERATURES IN ADVANCED MATERIALS



By
David L. Davidson
Kwai S. Chan
James Lankford

AFOSR ANNUAL REPORT FOR 1990

This research was sponsored by the Air Force Office of Scientific Research,
Electronic and Materials Sciences Directorate
Under Contract F49620-89-C-0032
Approved for release; distribution unlimited.

January 1991



SOUTHWEST RESEARCH INSTITUTE
SAN ANTONIO
DETROIT
HOUSTON
WASHINGTON, DC

SECURITY CLASSIFICATION OF THIS PAGE

REPORT DOCUMENTATION PAGE				Form Approved OMB No. 0704-0188 Exp. Date: Jun 30, 1999
1a. REPORT SECURITY CLASSIFICATION UNCLASSIFIED		1b. RESTRICTIVE MARKINGS		
2a. SECURITY CLASSIFICATION AUTHORITY		3. DISTRIBUTION/AVAILABILITY OF REPORT		
2b. DECLASSIFICATION/DOWNGRADING SCHEDULE		Approved for public release; distribution unlimited		
4. PERFORMING ORGANIZATION REPORT NUMBER(S) 06-2699/2		5. MONITORING ORGANIZATION REPORT NUMBER(S) F49620-89-C-0002		
6a. NAME OF PERFORMING ORGANIZATION Southwest Research Institute		6b. OFFICE SYMBOL (If applicable)	7a. NAME OF MONITORING ORGANIZATION Air Force Office of Scientific Research	
6c. ADDRESS (City, State, and ZIP) 6220 Culebra Road San Antonio, TX 78228-0510		7b. ADDRESS (City, State, and ZIP Code) Department of the Air Force Bolling Air Force Base Washington, D.C. 20332		
8a. NAME OF FUNDING/SPONSORING ORGANIZATION AFOSR		8b. OFFICE SYMBOL (If applicable)	9. PROCUREMENT INSTRUMENT IDENTIFICATION NUMBER F49620-89-C-0039	
8c. ADDRESS (City, State, and ZIP) Department of the Air Force Bolling Air Force Base Washington, D.C. 20332		10. SOURCE OF FUNDING NUMBERS		
		PROGRAM ELEMENT NO. 61102F	PROJECT NO. 2306	TASK NO. A1
11. TITLE (Include Security Classification) Crack Growth Processes at Elevated Temperatures in Advanced Materials				
12. PERSONAL AUTHOR(S) D. L. Davidson, K. S. Chan, and J. Lankford				
13a. TYPE OF REPORT Annual		13b. TIME COVERED FROM 1/1/80 TO 1/1/81	14. DATE OF REPORT (Year, Month, Day) 91/01/31	15. PAGE COUNT
16. SUPPLEMENTARY NOTATION				
17. COSATI CODES			18. SUBJECT TERMS (Continue on reverse if necessary and identify by block number)	
FIELD	GROUP	SUB-GROUP	Key Words: titanium aluminide alloy, fatigue crack growth, fracture toughness	
19. ABSTRACT (Continue on reverse if necessary and identify by block number)				
<p>The role of alloying on fatigue crack growth through titanium alloys has been previously investigated for the $\alpha + \beta$ and $\alpha_2 + \beta$ alloys. This work has now been extended to $\alpha_2 + \gamma$ alloys through experiments with alloys based on TiAl. Fatigue cracks were grown at 800°C through a lamellar $\alpha_2 + \gamma$ alloy, and some work was also done at ambient temperature. Crack tip micromechanics measurements were made the mechanisms of fatigue crack growth were investigated by direct observation of crack growth using a cyclic stage in the scanning electron microscope.</p> <p>Direct measurements of fatigue crack closure were made for center notched specimens of the aluminum alloy 7091, and these were compared to similar measurements from single edge notched specimens of the same alloy. The results indicate that plasticity induced closure can be treated in a systematic way and is linked to the threshold for fatigue crack growth. A simple model was developed which can be used to simulate the opening of fatigue cracks. These results were then compared to similar information from stainless steel, aluminum, and titanium alloys. Some general conclusions about closure were identified.</p> <p>The roles of microstructure in the fracture toughness and tensile ductility of the two-phase Ti₃Al-base and TiAl base alloys were established by identifying the relevant fracture and toughening processes in these alloys by performing crack-tip micromechanics experiments both at ambient and elevated temperatures. Additionally, strain distribution within the crack-tip plastic zone was measured using the machine-vision-based stereovision technique. The in-situ observations of the near-tip fracture processes and strain measurements were used in conjunction with micromechanical modeling to distinguish the various roles of microstructure in the fracture and toughening mechanisms, and to establish microstructure/toughness relationships in these representative two-phase titanium aluminide alloys.</p>				
20. DISTRIBUTION/AVAILABILITY OF ABSTRACT			21. ABSTRACT SECURITY CLASSIFICATION	
<input checked="" type="checkbox"/> UNCLASSIFIED/UNLIMITED <input type="checkbox"/> SAME AS RPT. <input type="checkbox"/> DTIC USERS			UNCLASSIFIED	
22a. NAME OF RESPONSIBLE INDIVIDUAL <i>Davidson</i>			22b. TELEPHONE (Include Area Code) 202 767-4983	22c. OFFICE SYMBOL NE

TABLE OF CONTENTS

	Page
I. RESEARCH OBJECTIVES	1
II. MATERIALS	2
III. FATIGUE	3
A. Fatigue Crack Closure	3
B. Titanium Aluminides	29
IV. FRACTURE TOUGHNESS	41
A. Microstructure/Toughness Relationships in Two-Phase ($\alpha_2 + \beta$) Titanium Aluminide Alloys	41
B. Microstructure/Toughness Relationships in Two-Phase Gamma Titanium Aluminide Alloys	49
C. Overall Assessment of Ductile Phase Toughening in Two-Phase Titanium Aluminide Alloys	61
V. REFERENCES	62
VI. PUBLICATIONS	66
VII. PROGRAM PERSONNEL	67
VIII. INTERACTIONS	68

Accession For	
NTIS CRA&I	<input checked="" type="checkbox"/>
DTIC TAB	<input type="checkbox"/>
Unannounced	<input type="checkbox"/>
Justification	
By	
Distribution /	
Availability Codes	
Dist	Available and/or Special
A-1	

LIST OF FIGURES

Figure		Page
1	The dependence of $U = \Delta K_{\text{eff}}/\Delta K_{\text{max}}$ for a center notched specimen of 7091 aluminum alloy.	19
2	Applied load normalized by opening load as a function of the distance from the actual to the crack tip open in Mode I for a center notched specimen of 7091. One micrometer has been added to the length of open crack so that the opening load can be included. The line shown is eq. (4). Part of the cracks analyzed are shown in this figure and the remainder are shown in Fig. 3.	20
3	Normalized load as a function of d (the closed crack length) for the 7091 center notched specimen. The opening load has been included by adding $1 \mu\text{m}$ to d . The line shown is eq. (4). This is an extension of Fig. 2.	21
4	Normalized load as a function of $d + 1$ for the single edge notched specimen of 7091. Compare with Figs. 2 and 3. The line shown is eq. (4).	22
5	Comparison between a simulation of crack opening using a finite element model and experimental data for a center notched specimen of 7091 aluminum alloy.	23
6	Comparison between a simple model for crack closure developed in the text and experimental data for 7091 aluminum alloy.	24
7 (a)	Closure measurements for SEN specimens of 7091 aluminum alloy. Comparison of direct measurements [10] to those using a crack mouth gauge [32].	25
7 (b)	Closure values determined by direct measurements from SEN specimens of 7091 aluminum alloy by assuming that the crack tip was the distance shown behind the actual tip. By assuming the crack tip was $\approx 500 \mu\text{m}$ behind the actual location, results from the crack mouth gauge were simulated.	25
8	The dependence of $U = \Delta K_{\text{eff}}/\Delta K$ on $1/K_{\text{max}}$ for SEN specimens of sensitized 304 stainless steel in an aqueous environment at 90°C .	26
9	The dependence of $U = \Delta K_{\text{eff}}/\Delta K$ on $1/K_{\text{max}}$ for SEN specimens of titanium alloys. (a) CORONA-5 and (b) 2411.	27
10	The dependence of $U = \Delta K_{\text{eff}}/\Delta K$ on $1/K_{\text{max}}$ for SEN specimens of particulate SiC reinforced 2014 aluminum alloy composite.	28

LIST OF FIGURES (cont'd)

Figure		Page
11	Fatigue crack growth rates for TiAl alloy at ambient and 800°C.	35
12	Photographs of the crack tip showing the growth of a fatigue crack in TiAl alloy at 800°C, $\Delta K = 17 \text{ MPa}\sqrt{\text{m}}$. Sequence starts in (a) at 0 cycles, and the number of cycles for each of the subsequent photographs is shown in the lower left of the figure. Note how tight the crack closes at minimum load, as shown in (h).	36
13	Crack length (a) vs number of cycles, and crack growth rate (b) vs crack length for the crack growth shown in Fig. 12.	37
14	Crack tip opening displacement (CTOD) at crack tip strain vs ΔK_{eff} for fatigue cracks grown in the TiAl alloy at 800°C.	38
15	Crack tip strain vs CTOD for fatigue cracks grown in the TiAl alloy at 800°C.	39
16	Microstructures of Ti-24Al-11Nb: (a) equiaxed $\alpha_2 + \beta$ microstructure; (b) coarse basketweave microstructure of $\alpha_2 + \beta$ platelets; and (c) fine basketweave microstructure of $\alpha_2 + \beta$ (insert) with primary α_2 platelets.	40
17	Typical equiaxed (a), coarse basketweave (b), and fine basketweave (c) microstructures.	43
18	Comparison of J-resistance curves for the equiaxed, coarse basketweave, and fine basketweave microstructures of the Ti-24Al-11Nb alloy at 25°C.	45
19	Comparison of J-resistance curves for the equiaxed, coarse basketweave, and fine basketweave microstructures of the Ti-24Al-11Nb alloy at 600°C.	46
20	Composite in-situ SEM micrographs showing the near-tip fracture process in the coarse basketweave microstructure is characterized by blunting of the tips of the main crack and microcracks by the continuous β phase. The volume of β is 39%.	47
21	Composite in-situ SEM micrographs showing the near-tip fracture process in the fine basketweave microstructure is characterized by propagation of the main crack around and through the smaller, discontinuous β phase. The volume fraction of β is 25%.	48
22	Comparison of calculated initiation toughness (K_{Ic}) with measured values from this study and those from Soboyejo et al. [25] and DeLuca et al. [26]. The result of Rowe et al. [27] for single phase α_2 Ti-24Al-7.5Nb alloy was used as an input to the crack-tip blunting model.	50

LIST OF FIGURES (cont'd)

Figure		Page
23	Microstructures of G1F (a, c) and G1L (b, d) showing: fine gamma grains in optical micrograph (a) with grain boundary alpha-2 phases imaged bright in the back-scattered electron image (c); large lamellar grains (b) consisting of alternative layers of gamma plates and alpha-2 plates (d) with fine grain boundary gamma. The alpha-2 plates in the lamellar structure are imaged light in the back-scattered electron image (d).	53
24	Comparison of the K-resistance curves for the lamellar microstructure at various test temperatures. The lamellar microstructure exhibits higher K_{Ic} values and crack growth resistance both at ambient elevated temperatures, when compared to the equiaxed γ microstructure.	54
25	Composite in-situ SEM micrographs showing the near-tip fracture process in the Ti-47Al-2.6Nb-2(Cr + V) alloy: (a) fracture by grain boundary decohesion in the equiaxed γ microstructure; (b) fracture by translamellar and apparent interface propagation with microcrack formation in the lamellar microstructure.	55
26	Near-tip effective strain measurements showing higher strain values in the lamellar microstructure than in the equiaxed γ microstructure.	56
27	Composite in-situ SEM micrographs showing the near-tip fracture process in the lamellar microstructure at 800°C is characterized by apparent interface growth and translamellar propagation along localized shear bands.	58
28	Comparison of the measured effective strain distributions with the HRR theory at two K levels showing lower measured strain values at a given K level. The discrepancy suggests that the near-tip K values are lower, probably due to the presence of one or more shielding mechanism(s) operative near the crack tip.	59
29	Comparison of engineering stress-strain curves for the lamellar microstructure tested at 800°C in air and in vacuum.	60

LIST OF TABLES

Table		Page
1	Closure Measurements	6
2	Estimates of ΔK_{th} (MPa \sqrt{m})	13
3	Crack Tip Parameters	32
4	Summary of Tensile, Fracture and Microstructural Properties of Ti-24Al-11Nb	44
5	Heat-Treatment Procedures, Microstructures, Tensile, and Fracture Properties of the Near Gamma Alloy, Ti-47Al-2.6Nb-2(Cr + V)	51

I. RESEARCH OBJECTIVES

Determining the mechanisms of fatigue crack growth and fracture toughness and developing microstructurally based quantitative descriptions of these processes for alloys based on the intermetallic compound TiAl were the principal objectives of research for last year. These objectives were accomplished by performing ambient and elevated temperature fatigue and fracture toughness experiments both using conventional techniques and the Southwest Research Institute developed scanning electron microscope cyclic loading stages, and the stereoimaging technique for measuring displacements.

Fatigue cracks were initiated in these materials, followed by studies of crack growth and crack tip mechanics from near-threshold stress intensity factors to the point of growth instability at ambient temperature and 800°C. The role of microstructure in the fracture mechanisms and toughness response was evaluated for two contrasting microstructures at ambient and elevated temperatures up to 800°C.

Fatigue crack closure measurements for the TiAl alloy was complemented by measurements for the aluminum alloy 7091. Crack opening loads were determined by direct measurements at the crack tip for cracks grown in center notched specimens. Measurements for this geometry were compared to extensive data collected from cracks in single edge notched specimens previously. These results were compared to similar measurements for other alloys including titanium alloys. From the collective information of all these closure data, some general conclusions were drawn about the nature and origin of closure.

II. MATERIALS

The materials to be investigated in this program were the titanium and niobium aluminides. During the first year, emphasis was on the Ti_3Al based alloy designated 2411, while during the past year the emphasis was on a TiAl alloy, with some work begun on a Nb_3Al based alloy.

Most of the research was performed on the TiAl based alloy which was obtained through Dr. Young Won Kim with Metcut Materials Research Group at Wright-Patterson AFB, Ohio. This material, designated G1, had the composition Ti-47.0Al-0.93Cr-0.85V-2.6Nb (atomic percent) with impurities of 550 O, 55 N, 160 C and 14 ppmw H. More information on heat treatments and material characterization will be given in later sections.

The Nb_3Al based alloy was supplied by Dr. Donald Anton of United Technologies Research Laboratory. Composition characterization of this material is incomplete at this time. Specimens have been machined from this material, fatigue precracked, and are being prepared for further testing.

III. FATIGUE

A. Fatigue Crack Closure

Background

Fatigue crack closure, since its discovery by Elber [1], has been one of the most intensely studied parameters associated with fatigue crack growth. But despite all the experimental measurements of closure and the theoretical models advanced to explain these observations, fatigue crack closure remains a poorly understood phenomena. A measure of the complexity of closure can be derived from the 1989 conference proceedings "Fatigue Crack Closure" [2]. The wide spectrum of results presented in that conference seems to indicate that closure is not a rationally determinable quantity, and, therefore is unlikely to be predictable. One purpose of our work on closure is to determine if closure can be predicted, or if this parameter must always be measured.

Reinforcing the seemingly chaotic nature of fatigue crack closure is the report on multi-laboratory measurements of closure by ASTM Task Group E24.04.04 [3]. Data from the round robin tests on the same specimen geometry and material exhibited large differences depending which laboratory, investigator, and technique were used. One of the conclusions drawn from this work was that:

"... scatter of this magnitude would make it very difficult to develop a clear picture of closure effects and to verify quantitative models of closure effects using data from the literature."

However, these results are not too surprising in light of reports that the level of closure depend upon where the measurement is made [4,5]. Adding to the confusion over measurement technique, Horng and Fine [6] and Vecchio, et al. [7] have found that closure is also dependent on the geometry of the specimen being tested.

The results presented first examine the variation of crack closure with stress intensity factor and specimen geometry for the aluminum alloy 7091. The results of measurements from center notched (CN) specimens of 7091 are compared with those obtained from single edge notched (SEN) specimens of the

same alloy. A single framework is presented which encompasses both geometries studied. No specimen geometry and alloy effects were found on general closure characteristics, but quantitative differences in closure level have been measured. A simple model is presented which approximates the experimental results and assists in their interpretation.

Finally, the results for 7091 aluminum alloy are compared to similar measurements for other aluminum alloys, titanium alloys, composites and stainless steel, all of which show similar behavior.

Experimental Technique

A fatigue crack grown under constant amplitude conditions at low homologous temperature is closed over most of its length at minimum cyclic load, at least when $R (P_{\min}/P_{\max}) \leq 0.4$. A fatigue crack at minimum load has material on both sides in very close contact, so close, in fact, that it is often difficult to detect the crack path and determine the location of the crack tip. As load is applied, the open portion of crack increases until, at P_0 , the crack is fully open to the tip. This process is easily observed by loading cracked specimens inside the scanning electron microscope using a special cyclic loading stage designed to fit in the specimen chamber [8].

Photographs in the region of the crack made at minimum load may be compared in a stereoscope with photographs of the same region made at progressively larger loads. By this comparative technique, the open portion of the crack may be visualized and directly measured from photographs using an ordinary graduated scale. As the open portion of the crack approaches the crack tip, higher magnification photographs increase the accuracy of the measurement, so that the load at which the crack actually opens can be determined very accurately. This technique can also be used in conjunction with optical microscopy, but experience has shown that the accuracy with which opening load can be determined is diminished, especially at low R , due to the limits in resolution imposed by optical microscopy. When cracks are viewed in the stereoscope with the crack oriented perpendicular to the eye axis, the Mode I opening is seen; when the crack is oriented parallel to the eye axis, the Mode II opening, or sliding, is seen.

This technique for measuring opening has been used on many materials

over a long time period; thus, considerable experience has been gained with its use. Numerous observations have shown that if opening loads are measured repeatedly for a crack being grown under conditions of constant cyclic stress intensity factor (ΔK), there is a variation in opening load which is greater than the uncertainty in the measurements. These changes in opening load are similar to the non-repeatability of the events accompanying fatigue crack growth when it is observed dynamically under high resolution conditions [9]. Thus, for a given ΔK level, several measurements are necessary to obtain a representative value of the opening load. The closure data taken with this technique from SEN specimens for several materials were the result of many measurements [10,11,12]. With the trends for aluminum alloy SEN specimens well established, fewer measurements are required for other geometries and materials in order to establish the extent to which observed closure behavior can be generalized.

The CN specimen used had a gage section of 19 mm and was 3 mm thick. The alloy, designated 7091-T7E69, was purchased from Alcoa in about 1979. This material is a powder metallurgy product, having a grain size of about 5 μm , and a yield stress of approximately 500 MPa (0.2% strain offset)[13]. Through thickness cracks were grown perpendicular to the rolling direction from a center notch introduced by a thin slitting saw. The crack was initiated at $\Delta K \approx 6 \text{ MPa}\sqrt{\text{m}}$ and was down loaded to $\Delta K \approx 3.0 \text{ MPa}\sqrt{\text{m}}$ after the crack had grown approximately 1.6 mm ($2a = \text{total crack length}$). For all crack growth, $R = 0.1$. Threshold ΔK for this material, measured from a SEN specimen, is approximately 1.7 $\text{MPa}\sqrt{\text{m}}$ [13]. Load level was then increased in small increments ($\approx 12\%$) as the crack lengthened, until the maximum ΔK of the experiment was reached ($2a = 11 \text{ mm}$). Stress intensity factors were determined using the relations derived by Gray [14]. Crack growth was not symmetrical about the specimen centerline, so the relations derived by Gray for an asymmetric crack were used to compute ΔK at each end of the crack based on measured length of the half crack. Measurements were made from both sides (A and B) and from both crack tips (Left and Right).

Results

Two quantities were measured for the CN specimen as a function of crack length and load. The length of the closed crack, d , was determined with increasing load, P , and the opening load, P_o , was measured in Mode I. It was

noted that there was considerably less Mode II crack opening for these experiments than previously observed for SEN specimens [15]. Some P vs d data for the SEN specimen were taken previously [11], and these will be compared to present results, but the main comparison with SEN data will be in terms of effective stress intensity factor, ΔK_{eff} , which is derived from the opening load, P_o .

Crack Opening Load

Measured Mode I opening loads varied between 1100 and 1650 N; these data and other important parameters are given in Table 1. The last column of the table gives the value of $U = \Delta K_{\text{eff}}/\Delta K$ for Mode I computed from the opening and maximum loads using the relation

$$U = (1 - P_o/P_{\text{max}})/(1-R) \quad (1)$$

which is derived directly from the definitions of $\Delta K_{\text{eff}} = K_{\text{max}} - K_o$, and R .

Table 1
Closure Measurements

Measurement	Crack tip	K_{max} (MPa $\sqrt{\text{m}}$)	P_{max} N	P_{open} N	U
1	BL	3.0	1445	1400	0.044
2	BR	3.55	1445	1400	0.033
3	AL	4.3	1445	1150	0.222
4	BR	4.9	1914	1350	0.32
5	AR	5.0	1445	1200	0.19
6	AL	7.0	1914	1110	0.47
7	BL	8.8	2990	1650	0.50
8	BR	10.2	2990	1100	0.70
9	AL	19.0	2990	1400	0.59

During our previous work on closure, Hudak discovered a correlation between U and $1/K_{\text{max}}$ for closure data from SEN specimens [10]. Data from the CN specimen are shown using this same format in Fig. 1. The line drawn

through this data is a least squares fit which has been forced through $U = 1$ at $1/K_{\max} = 0$, and has the equation ($R = 0.1$)

$$U = 1 - 3.32/K_{\max} \quad (2)$$

which may be compared to that derived from the SEN specimen ($0.1 < R < 0.8$) [10]

$$U = 1 - 5.0/K_{\max} \quad (3)$$

The form of the closure results is clearly similar for SEN and CN specimens, although the slopes of the lines are different.

Progressive Opening of the Crack

The length of closed crack (d) is correlated with P/P_0 in Figs. 2 and 3. These are representative data; all of the measurements made are not shown. In order to include the crack tip ($d = 0$) on the logarithmic scale, $1 \mu\text{m}$ has been added to d . The function which has been found to approximately fit the data is

$$P/P_0 = 1 - m \ln(d+1) \quad (4)$$

where d is in μm and m is an empirically derived constant. Including all the measurements made gives $m = 0.11$. Note that eq. (4) is independent of K_{\max} over the range $3 < K_{\max} < 19 \text{ MPa}\sqrt{\text{m}}$.

Similar data for crack opening from SEN specimens of the same 7091 alloy have been published previously [10,11], and are shown for comparison in Fig. 4 using the same format as used for Figs. 2 and 3.

Progressive Closing of the Crack

Some observations have been made during the unloading portion of the fatigue cycle to determine how cracks close for both the SEN and CN geometries. Other investigators have reported that sometimes the crack flanks touch at some distance behind the tip before closure occurs at the crack

tip itself [16, 17]. We have not seen this behavior for cracks in either CN or SEN specimens. Careful observations indicate that the crack closes first at the crack tip and then progressively back along the crack flanks opposite to the way it opened, although the loads at which the crack is closed to any specific distance behind the tip are lower than those when the crack is in the opening mode with increasing load.

Modeling

There have been a number of analytically derived models for crack closure, as well as numerous finite element simulations. Rather than review or reference all of these, the reader should consult McClung and Sehitoglu [18], who have also compared the predictions of each. For $R = 0$, finite element simulation predicts $0.54 < P_o/P_{max} < 0.62$, irrespective of the level of ΔK , but strongly dependent on σ_{max}/σ_{ys} , the ratio of applied stress to yield stress. In the present experiments, σ_{max}/σ_{ys} levels did not exceed 0.12, and were mostly less than about 0.08. For this small of a change, simulation would predict practically no change in P_o/P_{max} .

McClung has used finite element modeling to simulate a crack growing under cyclic loading [19]. There is agreement between the simulation and several of the experimentally measurable parameters, including the strain distribution ahead of the crack tip and the relationship between crack opening displacement and distance behind the crack tip. Sequential opening of the crack has been examined also using this model, and the results are shown in Fig. 5. In making this comparison, the length of closed crack was nondimensionalized. The factor $(K_{max}/\sigma_{ys})^2$ was chosen because it was used successfully for nondimensionalization when modeling other aspects of fatigue crack growth. The finite element model simulates the experimental result fairly well, even though the opening data for the center notched specimen do not collapse to a single line on the basis of the nondimensionalizing parameter chosen.

Many analytical models, typified by the works of Budianski and Hutchinson [20], use some form of the Dugdale strip yield concept, with displacements at the crack tip being carried into the crack wake as the crack tip passes. The mathematics of the models using this approach are complex

and it has not been determined what alterations could be made in them to better agree with our experimental results. Therefore, a more direct modeling approach was sought which would agree with experiment and which would be easier to understand. It was recognized at the outset, however, that a simple model was unlikely to include all of the factors which might govern closure. The objective of the model developed here was to simulate a sequential opening of the crack with applied load, as measured and depicted in Fig. 2,3 and 5.

The modeling procedure finally implemented uses the analysis of Tada et al. [21], which computes the crack tip stress intensity factor caused by point loads applied at locations within the specimen. For purposes of defining the location of these point loads, the crack tip is used as the origin. The point load P_r is applied at an angle θ to the crack plane, and at a distance r_o away from the tip. The Mode I stress intensity factor K_r caused by each load P_r is

$$K_r = P_r [\alpha \sin\theta \cos(3\theta/2) - 2\sin(\theta/2)] / \sqrt{2\pi r_o} \quad (4)$$

where $\alpha = 1/2(1-\nu) \approx 1/3$ for plane strain. Thus, the point load causes a stress intensity factor which is directly proportional to its magnitude and inversely proportional to the square root of its distance from the crack tip. The geometric factor [within brackets] indicates that the load has no effect ($K_r = 0$) when it is applied along the crack plane ($\theta = 0^\circ$), and maximum effect for $\theta \approx 125^\circ$. If more than one load is applied, then the stress intensities of each are additive. Thus, a distributed load may be represented by one value applied at the centroid of the loaded region.

The present model uses two symmetrical point loads to simulate a number of possible mechanisms which could be responsible for crack closure, including (1) residual stress within the crack tip plastic zone, and (2) stretching of material in the crack wake caused by irreversible plasticity as the crack tip passes. This model relates crack closure to K_r , which is similar to the concept used in some computer simulations of crack tip plasticity, in that a stress intensity of some magnitude (K_D) must be overcome before dislocations can be emitted from the crack tip [22]. It has been shown also [23] that dislocations along the crack wake, simulating crack wake stretching, can produce this same effect.

For purposes of the present model, the point load is considered as a stress acting on a small area; thus, in concept, this load best represents a residual stress in the plastic zone forward of the crack tip. The other key assumption in the model is that the magnitude of this point load, or stress, is decreased in proportion to the magnitude of the applied stress, becoming zero at the opening load, so that

$$P_r = P_r(0)[1 - P_a/P_o] \quad (5)$$

where $P_r(0)$ is the value of P_r at minimum load and P_a is the applied load. Thus, the applied load is assumed to decrease the magnitude of the internal point load so that the point load is zero at opening load.

The procedure for computing the length of open crack as P_a is increased from minimum load is first to compute K_a at the crack tip caused by application of P_a , and from that, compute $K_{eff} = K_a - K_r$. The equivalent crack length is then determined from P_a and K_{eff} using the equation for stress intensity factor for the specimen geometry of interest

$$K_{eff} = \sigma_a \sqrt{\pi a'} F \quad (6)$$

where a' = length of open crack, σ_a = applied stress (P_a /area) and F = the geometric factor, as given by Gray [14].

When the simple procedure described above is applied, the crack is found to open sequentially, much as found experimentally. The model result is superimposed on some of the opening data in Fig. 6, where the best fit is seen to occur near the crack tip and the worst fit occurs remote to it. Values of the constants used were $\theta = 45^\circ$, $r_o = 1.25 \mu\text{m}$, and $P_r(0) = 130 \text{ N/m}$; the magnitudes of these factors have no actual physical meaning, except that they are of the correct magnitudes to represent a residual stress acting within the plastic zone of the crack tip. The general agreement between model and experiment indicates that the model has captured the essence of the physics underlying crack closure.

Comparison with Other Closure Data

Data for SEN specimens measured directly at the crack tip, as detailed above, are compared in Fig. 7(a) to closure levels measured remotely using a crack mouth clip gauge [10]. Knowledge of how the cracks open allows the direct measurements to be reinterpreted, assuming the crack tip is at a location behind the actual tip. Using this simple idea, the clip gauge results can be duplicated, as shown in Fig. 7(b). Thus, the remotely measured results obtained using the clip gauge are what would be obtained if the crack tip were assumed to be over 500 μm behind the actual location of the crack tip. This inaccuracy in measurement of crack opening loads by the remote technique may be attributed to the lack of sensitivity inherent in compliance measurements, and appears to be a major contributor to the lack of reproducibility in the ASTM committee results.

Crack closure data for 304 stainless steel measured over a large range of R ratio [10] are shown in Fig. 8. The data are seen to be described by eq. (3), with the slope of the line modified. Similar results are shown for the titanium alloys CORONA-5 and 2411 in Fig. 9. Closure levels have also been measured for fatigue cracks growing in an aluminum alloy matrix composite reinforced with SiC particles, as shown in Fig. 10 [24].

Discussion

Results from the CN specimen have the same form as for the SEN specimen of the same material, but the magnitudes of the closure are different, as indicated by eqs. (1) and (2). This same general result was also found for 304 stainless steel [10,25], even though much of the data of Staal and Elen [25] were obtained at high gross section stress. The similarity of closure measurements for all these materials and for both specimen geometries indicates that the origin of closure is the same.

The value of ΔK below which a fatigue crack will not grow is defined as ΔK_{th} . This condition occurs when $\Delta K_{eff} = 0$, therefore when $U = 0$. Thus, ΔK_{th} may be determined from the relation between U and K_{max} , as shown in Figs. 1 and 7-10. The importance of this finding is that the level of ΔK_{eff} , therefore the level of closure, can be determined from the simple relationship:

$$\Delta K_{\text{eff}} = \Delta K - \Delta K_{\text{th}} \quad (7)$$

which is just eq. (2) or (3) rewritten.

The importance of this relationship is that the level of crack closure and the magnitude of ΔK_{th} are linked. This result is intuitive, and has been used routinely to estimate ΔK_{eff} in fatigue analyses [26]. If ΔK_{th} could be computed, then the level of closure would be known at all levels of K for constant amplitude crack growth. In fact, it is possible to estimate ΔK_{th} , as will be indicated.

Yoder, et al. [27], made an analysis of variations in grain size and yield strength on the ΔK dependence of near-threshold fatigue crack growth, and found that an abrupt change in the relationship occurred at a distinct transition value, ΔK_T , which was proportional to the $\sigma_y \sqrt{l}$, where l was proportional to grain size. Their analysis is similar to that used previously by this author [12], and others [28,29], to predict ΔK_{th} . The relation needed to determine ΔK_{th} is derived from the theoretical elasticity relationship between stress intensity factor and stress ahead of a Mode I crack, which is

$$\Delta K_{\text{th}} = \sigma_y \sqrt{2\pi r_s} \quad (8)$$

where r_s is a distance ahead of the crack tip.

The simple assumptions used in estimating ΔK_{th} using this relation are:

(1) crack growth cannot occur without dislocation emission from the crack tip, (2) at ΔK_{th} , a slip line of length r_s emanates from the crack tip, and (3) the stress at the end of this slip line must rise to yield before dislocations can be emitted from the crack tip and move away, thereby allowing growth to occur (after sufficient damage accumulates). If the geometry or material allow appreciable Mode II opening to occur, a more accurate estimate of ΔK_{th} may be made by replacing σ_y with τ_y , the shear stress at yield. Thus, if shear at the crack tip is the dominant mode, then ΔK_{th} would be about half that estimated for Mode I opening.

The effect of R ratio on ΔK_{th} is not included in eq. (8) because this is the value at $R = 0$. For other values of R, the change in ΔK_{th} may be made through K_{max} , since the correlation of U is through K_{max} . Thus, eq. (8) for other values of R would be

$$\Delta K_{th} = (1-R) \sigma_y \sqrt{2\pi r_s} \quad (9)$$

For some materials, grain size may be the controlling microstructural parameter, but for the aluminum alloys, the mean free path of slip through the dispersoids was identified as the factor controlling slip [13]. This concept also was found to predict values of ΔK_{th} very well for aluminum alloys reinforced with SiC particles where the mean free path of dislocation motion could be determined with relatively good accuracy due to the presence of the SiC particles [30]. The general problem in using this concept to predict ΔK_{th} for other materials is in determining the relationship between the microstructure and the slip parameter r_s . Obviously, there are many factors such as grain size, particle size, slip character, and texture which could influence r_s , therefore, ΔK_{th} .

In addition to the values determined for the aluminum alloys and aluminum matrix composites, work has been done on alloys based on titanium and titanium aluminides. This work helps to further cement the relationship found between closure and threshold. The results of determinations of ΔK_{th} from crack growth rates, use of eq.(9), and from closure measurements for these alloys is shown in Table 2.

Table 2
Estimates of ΔK_{th} (MPa \sqrt{m})

<u>Method</u>	<u>2411</u>	<u>Super α2</u>	<u>CORONA-5</u>	<u>Ti-6Al-4V(RA)</u>
Crack growth rate	5.5 \pm 2	3.5 \pm 2	5.0 \pm 2	3.0 \pm 2
Mode 1 closure	5.8 \pm 0.5	not meas.	\approx 6.7	not meas.
Microstructure	4.0 \pm 0.5	4.0 \pm 0.5	6.6 \pm 1.5	4.5 \pm 1.0

One of the difficulties encountered in comparing values of ΔK_{th} determined from fatigue crack growth rate curves is that the value found depends on the technique and patience of the investigator. Specifically, if step downloading is used to determine ΔK_{th} , then the level of load reduction at each step is important. Thus, values of ΔK_{th} as determined from crack growth rate tests are not intrinsically more accurate than the value determined by either closure measurements or from microstructural parameters.

Horng and Fine [6] and Veccio, et al.[7], both determined that ΔK_{th} for the SEN specimen was greater than for CN, as was found in the present work. The explanation given for this by Horng and Fine was that crack closure was caused by fracture surface roughness, but that argument was disputed by Veccio, et al., who favored the concept that "microstructurally dominated crack growth will occur at higher ΔK levels for the SEN specimen than for the CN specimen" because the stress level is larger for the CN specimen than for the SEN specimen for a given level of K at a given distance from the crack tip. Their stress levels were determined by finite element analysis of the two specimen geometries. From this analysis, they determined that to reach a given level of stress ahead of the crack in the CN geometry, ΔK must be less than for the SEN specimen. Putting this difference in stresses into eq. (8) indicates that ΔK_{th} would be lower for the CN than for the SEN specimen, in agreement with all the measurements. A meaningful comparison cannot be made between the ratio of measured ΔK_{th} values and the ratio of stresses computed at a distance of $\approx 5-10 \mu\text{m}$ ahead of the tip because of the rapidly varying stress in that region, and because the finite element formulation used by Veccio, et al., did not have a mesh fine enough to give accurate results this close to the crack tip.

There is still controversy over whether plasticity induced crack closure is caused by residual stresses ahead of the crack tip or by material elongation in the wake of the crack. But, these two factors are not independent. Recent finite element work by McClung [19] suggests that closure is caused by both, with a nearly equal weight for each.

The model presented here can be interpreted similarly, in that point loads can be placed behind the crack to simulate wake effects, or ahead of the crack to simulate residual stresses in the plastic zone. Loads in both

locations translate into stress intensity factors at the crack tip which are additive. Thus, simulation of both wake stretch and residual stress in the plastic zone can be made by partitioning the point loads. It does not appear to be possible to use results obtained with the experimental techniques used here to apportion closure between these two factors.

The more important points associated with the present results are:

- (1) closure caused by either residual stress or crack wake effects can be represented by a stress intensity factor acting against that caused by the applied load, and
- (2) closure is linked to the threshold stress intensity factor for fatigue crack growth.

The first of these conclusions is supported by the modeling work, and the second is shown by the form of eqs. (1) and (2), which relate closure to ΔK_{th} .

The experimental technique of Suresh [31] showed that the existence of a ΔK_{th} is not just the result of improperly downloading a growing fatigue crack, i.e., intrinsic threshold does, in fact, exist. His technique used compression-compression loading to initiate the crack from a notch. The crack was then allowed to grow until it arrested under compression loading, which means that the crack tip was no longer generating any plasticity. Suresh showed that crack growth under subsequent loading in tension-tension required application of a minimum stress intensity factor, ΔK_{th} , which agreed reasonably well with the value of ΔK_{th} derived from careful downloading. This result implied that loading must be increased until some minimum in crack tip plasticity is reached. The model developed here for simulation of the crack opening also fits well with the observations made by Suresh.

Another complication associated with predicting ΔK_{th} is the transformation of the crack opening mode from predominantly Mode I at higher ΔK to mostly Mode II near ΔK_{th} [15], which occurs for the SEN specimen, but to a much smaller extent for the CN specimen. The reason for this dependence of Mode II on specimen geometry is unknown, but it could be as simple as the constraint against Mode II opening present for a CN specimen, but not for a SEN

specimen. A possible interpretation of the term ΔK_T of Yoder, et al. [27], is that ΔK_T represents the transition point between predominantly Mode I and Mode II opening. Since the values derived from eqs. (1) and (2) are determined only from Mode I opening, this would explain why these derived values are larger than threshold values determined from crack growth rate.

Hornig and Fine [6] also recognized that the near threshold region is characterized by mixed mode opening. They proposed that ΔK_{eff} be computed by combining two terms, one attributed to sliding (Mode II) and one attributed to opening (Mode I), with the proportion due to sliding increasing as ΔK was lowered. Using this concept, they were able to rationalize differences in crack growth rates between CN and SEN specimens, because SEN specimens have a larger Mode II component. This concept is corroborated by some measurements at ΔK values near threshold in SEN specimens, where values of opening load in Mode II were found to be larger than those for Mode I [11], which meant that the value for U was larger for Mode II than for Mode I.

It is well known that factors other than plasticity can greatly affect crack closure and ΔK_{th} . Environmental effects have been shown to be very important, with the main effect being formation of oxide in the crack near the tip. Present results indicate that it may also be possible to model oxide induced crack closure by representing oxide thickness by a stress intensity factor. The presence of hydrogen in the environment also affects crack growth rates and should have an effect on closure, which might be explained by the changes in the magnitude of the slip parameter, r_s , caused by hydrogen.

There is widespread belief that fracture surface roughness is an important factor in determining the level of closure. Hornig and Fine used the concept of roughness induced closure to explain their results, but Veccio, et al. make a convincing argument for why this need not be the cause of their results. In neither of these cases was there any quantitative measurement of surface roughness, and this is a general problem in attempting to examine the efficacy of roughness induced closure arguments.

The link between ΔK_{th} and crack closure provides one way of examining the relationship between roughness and closure. Roughness of fracture surfaces were measured for fatigue cracks grown very near threshold through

SiC reinforced aluminum alloys [30]. Surface roughness values showed no correlation with measured values of ΔK_{th} for these materials. Further experimental work is needed to provide quantitative assessment of the validity of roughness induced closure concepts, as well as to determine the level of closure caused by this mechanism relative to that caused by crack tip plasticity.

In our experiments with SEN and CN specimen geometries using the SEM loading stage, in only a very few instances have cracks been observed to close so that the crack surfaces meet without registry, thus wedging the crack open in the near vicinity of the crack tip. Disregistry in asperity contact has been observed several hundred micrometers behind the tip - a distance far enough away from the crack tip to have only minimal effect on closure. This observation was especially strong for Ti-6Al-4V(RA). For other materials and specimen geometries, or for conditions not yet studied, this mechanism cannot yet be dismissed as an important mechanism for closure.

Conclusions

1. Fatigue cracks peel open for center notched specimens (CN) just as was found for single edge notched specimens (SEN). Applied load, when normalized by opening load, shows an approximately linear-log relationship with the length of closed crack.
2. For Mode I opening of CN specimens, U ($\Delta K_{eff}/\Delta K$) is dependent on K_{max} through to the relation $U = 1 - K_o/K_{max}$, where $\Delta K_{eff} = K_{max} - K_{open}$ and $K_o = \Delta K_{th}/(1-R)$, at least for aluminum alloys. This is the same relationship as found for SEN specimens for several alloys and a particulate reinforced composite.
3. The relationship in (2) implies that for Mode I opening, $\Delta K_{eff} = \Delta K - \Delta K_{th}$. Thus, the level of closure is linked to the fatigue threshold. This relationship has been found in aluminum alloys both for SEN and CN specimens.
4. The level of closure was found to be different for the CN specimen than for the SEN specimen, in agreement with similar differences found by Horng and Fine [7] and Veccio, et al. [8].

5. A model which simulates crack opening is developed which uses residual stress in the plastic zone (or crack wake plasticity) to impose a stress intensity factor at the crack tip. Behavior of the model with applied load is similar to that found experimentally.
6. Experimental evidence and modeling suggest that the observed closure (thus ΔK_{th}) results from plasticity at the crack tip. Thus, ΔK_{th} is related to the minimum plasticity required to propagate a fatigue crack, which may be calculated in Mode I from the elasticity relationship $\Delta K_{th} = \sigma_y \sqrt{2\pi r_s}$, where r_s is the smallest slip distance which can occur in the material. If the material and specimen geometry allow a sizable Mode II opening, then a more accurate value of ΔK_{th} may be obtained by replacing σ_y with τ_y .
7. For the aluminum alloys studied, closure caused by crack roughness was not a factor, and the effects of oxides in the crack were minimal. The same is apparently true for aluminum alloys reinforced with SiC particles.

Acknowledgements

The author is grateful for the careful experimental work of John B. Campbell. Thanks also go to Dr. S.V. Harren for rewriting the equation of Tada [21] in algebraic form and to Dr. R.C. McClung for simulating the progressive opening of a fatigue crack with his finite element model and for helpful discussions on fatigue crack closure.

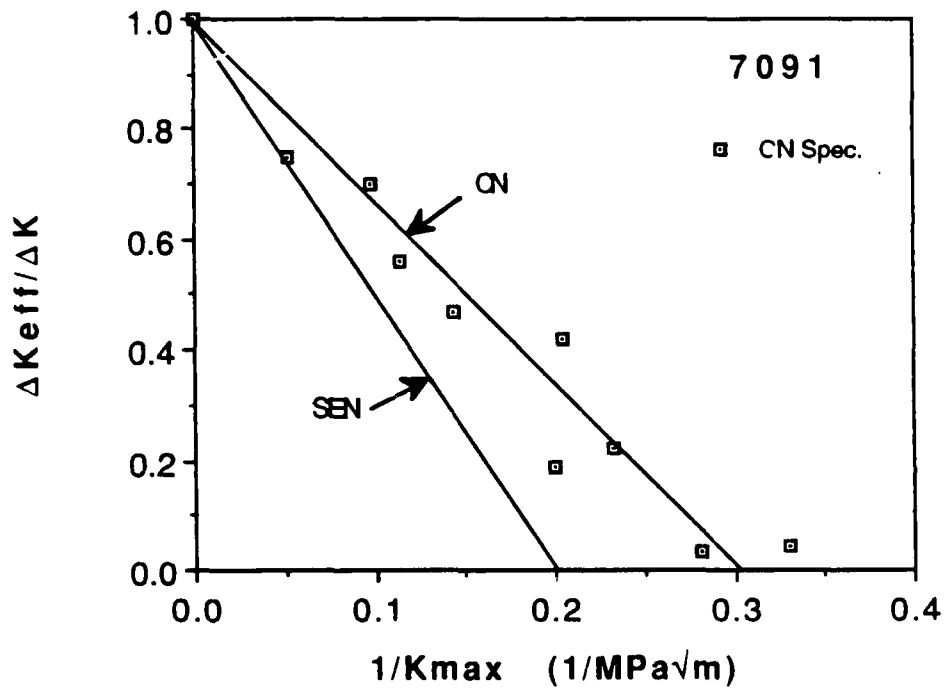


Fig. 1 The dependence of $U = \Delta K_{eff}/\Delta K$ for the center notched specimen on $1/K_{max}$, which is similar to that found for single edge notched specimens.

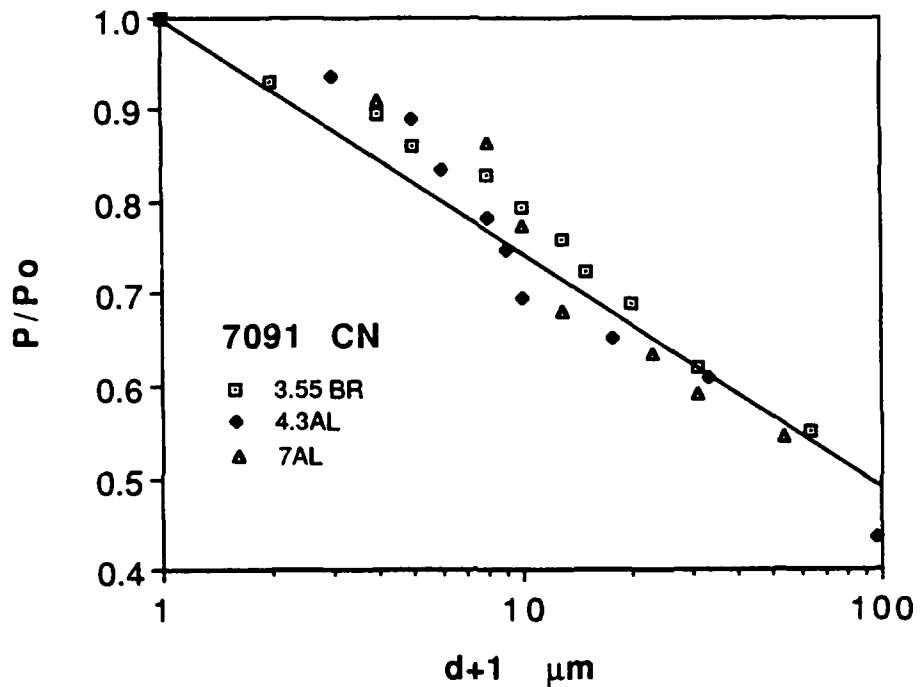


Fig. 2 Applied load normalized by opening load as a function of the distance from the actual to the crack tip open in Mode I for a center notched specimen of 7091. One micrometer has been added to the length of open crack so that the opening load can be included. The line shown is eq.(4). Part of the cracks analyzed are shown in this figure and the remainder are shown in Fig. 3.

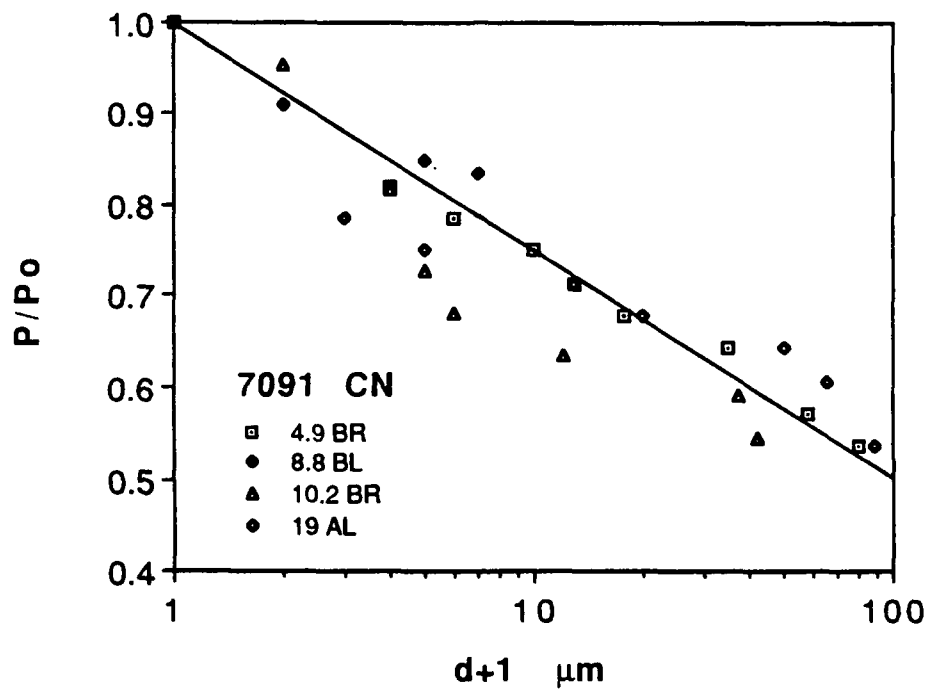


Fig. 3 Normalized load as a function of d (the closed crack length) for the 7091 center notched specimen. The opening load has been included by adding $1 \mu\text{m}$ to d . The line shown is eq.(4). This is an extension of Fig. 2.

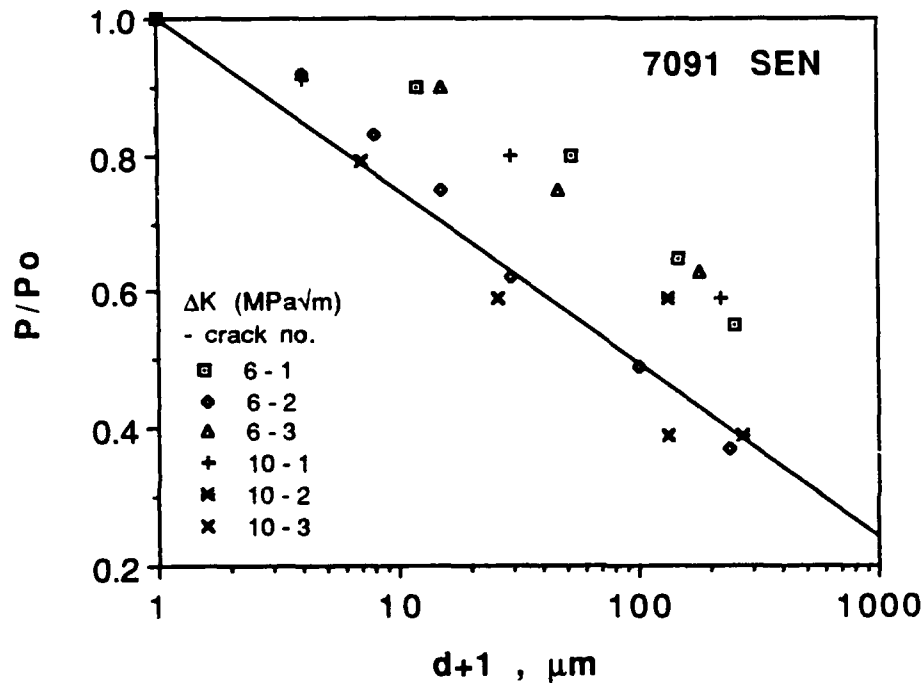


Fig. 4 Normalized load as a function of $d+1$ for the single edge notched specimen of 7091. Compare with Figs. 2 and 3. The line shown is eq.(4).

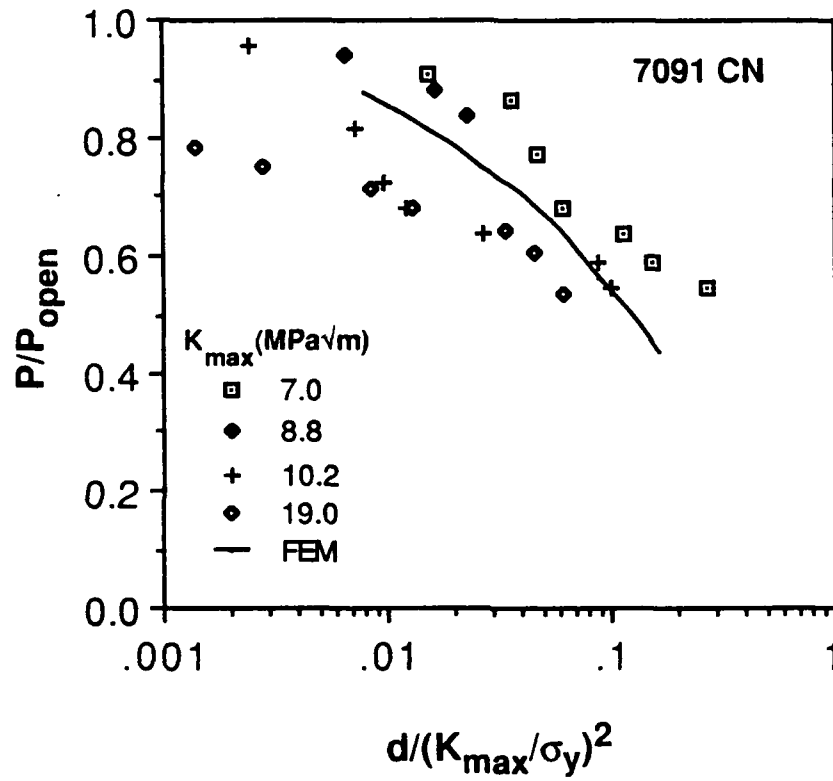


Fig. 5 Comparison between a simulation of crack opening using a finite element model and experimental data for a center notched specimen of 7091 aluminum alloy.

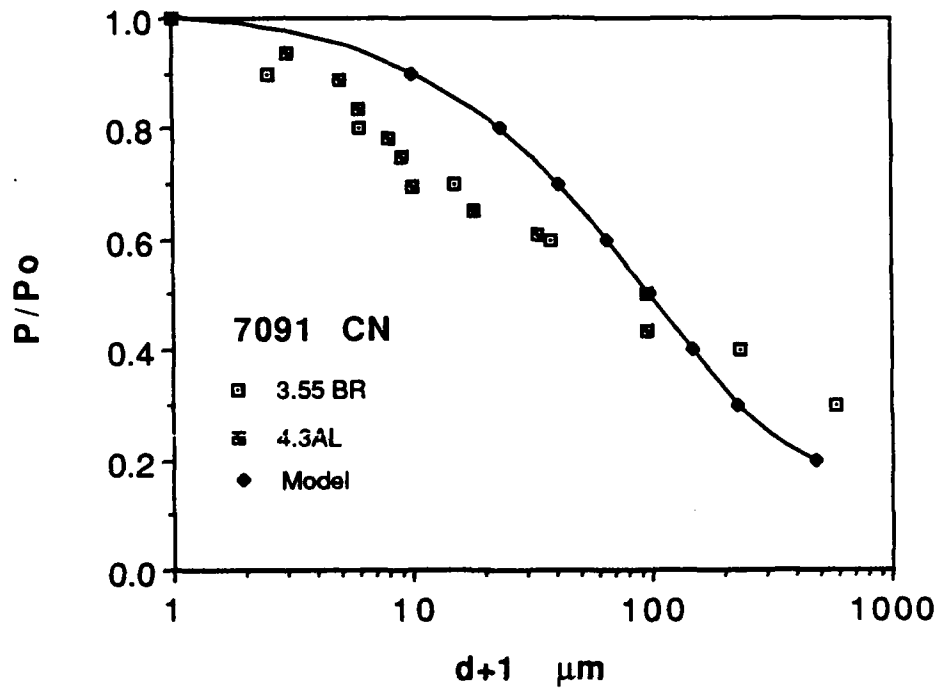


Fig. 6 Comparison between a simple model for crack closure developed in the text and experimental data.

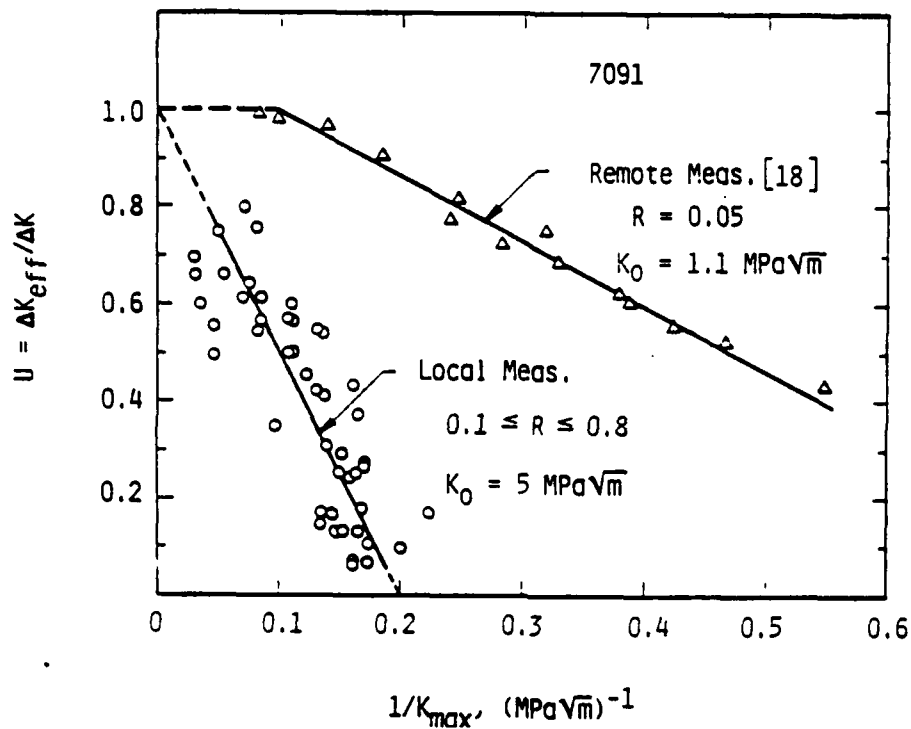


Fig. 7(a) Closure measurements for SEN specimens of 7091 aluminum alloy. Comparison of direct measurements [10] to those using a crack mouth gauge [32].

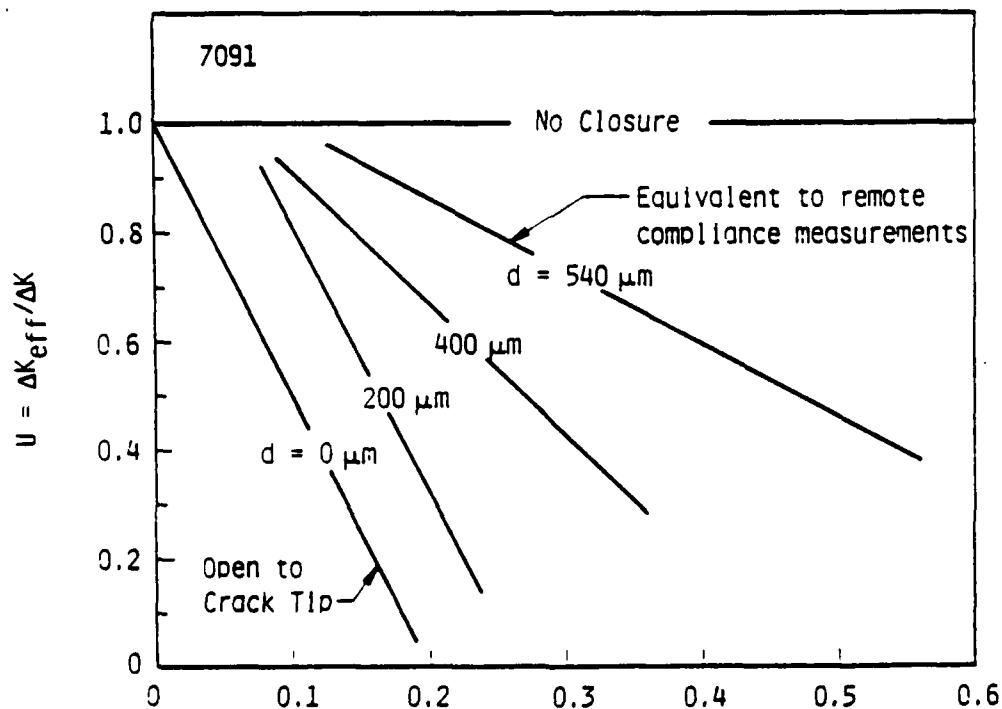


Fig. 7(b) Closure values determined by direct measurements from SEN specimens of 7091 aluminum alloy by assuming that the crack tip was at the distances shown behind the actual tip. By assuming the crack tip was $\approx 500 \mu\text{m}$ behind the actual location, results from the crack mouth gauge were simulated.

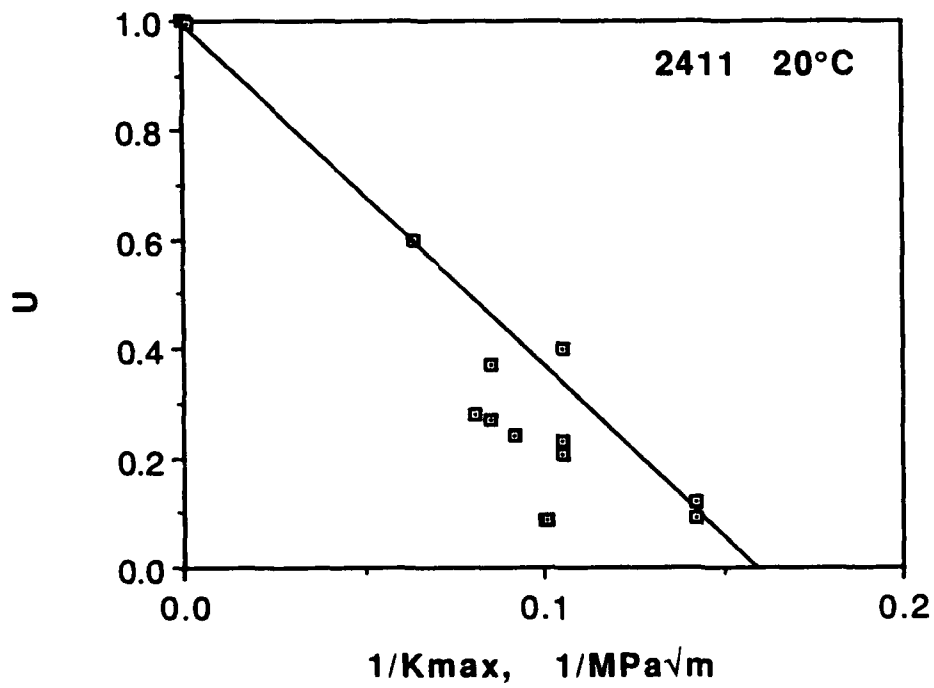
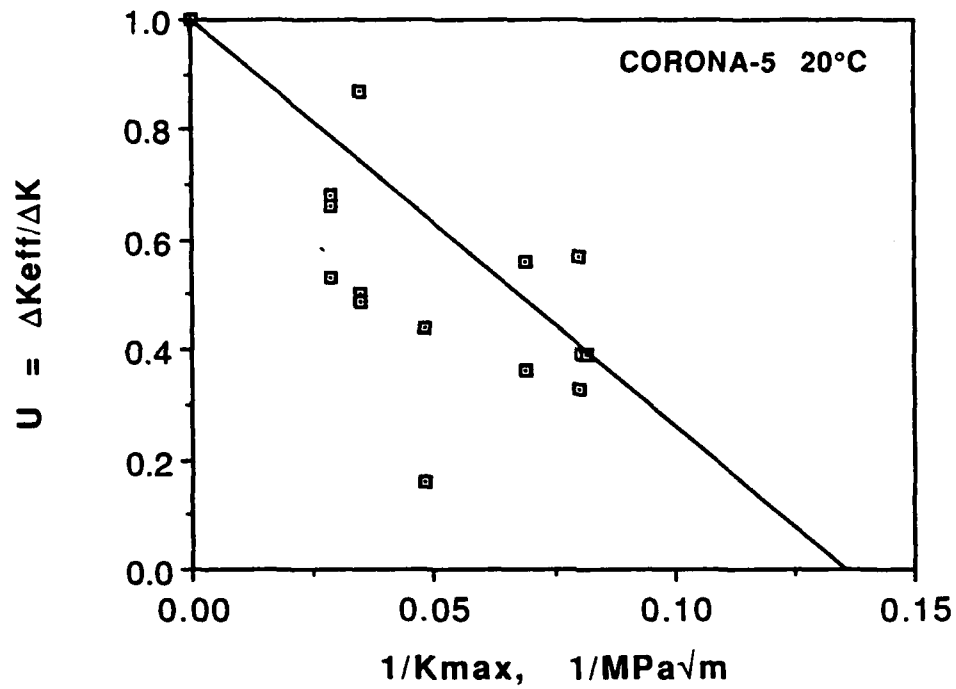


Fig. 9 The dependence of $U = \Delta K_{eff}/\Delta K$ on $1/K_{max}$ for SEN specimens of titanium alloys. (a) CORONA-5 and (b) 2411.

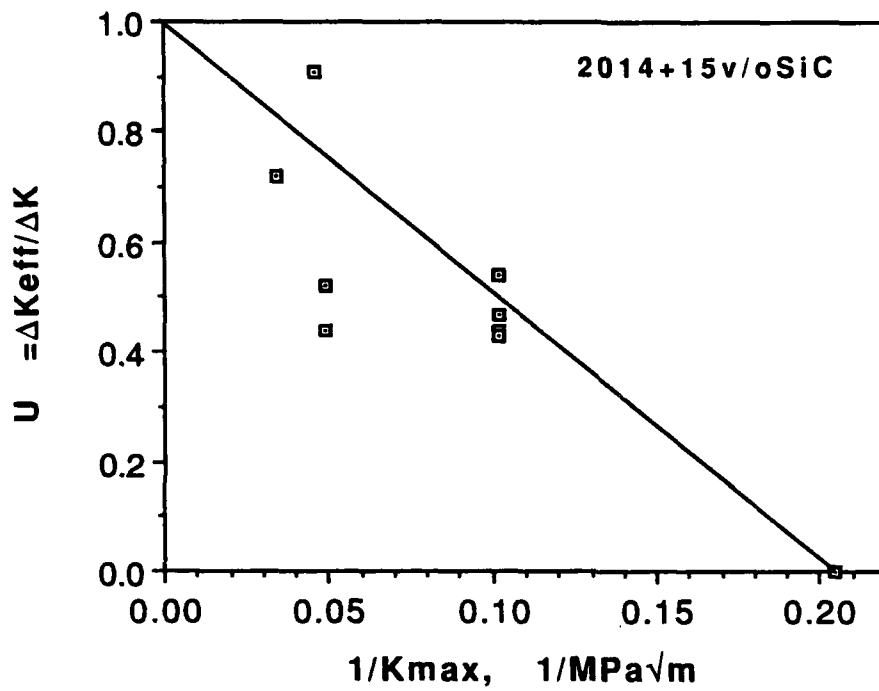


Fig. 10 The dependence of $U = \Delta K_{eff}/\Delta K$ on $1/K_{max}$ for SEN specimens of particulate SiC reinforced 2014 aluminum alloy composite.

B. Titanium Aluminides

Background

The mechanisms and micromechanics of fatigue crack growth at ambient temperature through two $\alpha+\beta$ titanium alloys, Ti-6Al-4V (RA) and CORONA-5, and two $\alpha_2+\beta$ titanium aluminide alloys, Super Alpha 2, and 2411, were examined and compared [33]. The mechanisms of fatigue crack growth through these alloys were typified more by their similarity than by their differences. In all cases, for crack growth near threshold, a large number of cycles (ΔN) was required before the crack lengthened (Δa). The sequence of events accompanying crack extension was observed to be similar to those found for aluminum alloys; a sharp crack blunted as the number of cycles increased, followed by crack extension and resharping. For the $\alpha+\beta$ alloys, slip lines were observed to form at the crack tip during the blunting process, and crack advance occurred by breakdown of this slip line. For the $\alpha_2+\beta$ alloy 2411, crack blunting was observed also, but often an α_2 particle near the crack tip broke, and crack advance occurred by linking of this broken particle with the main crack tip.

All the alloys examined to date have had varying amounts of β phase in the microstructure, and all have been approximately equiaxed. A fundamentally different microstructure has been examined during the past year in the TiAl alloy system $\alpha_2+\gamma$. The material, obtained from Dr. Young Won Kim of Metcut Materials Research Group, had the nominal composition (at.%) of Ti-47Al-0.9Cr-0.8V-2.6Nb. Processing resulted in a microstructure of mostly lamellar plates of α_2 and γ with some regions of equiaxed γ , as will be illustrated in one of the figures. Fatigue cracks were grown through this material at 20 and 800°C.

The results to date have been mainly for crack growth at 800°C because it has been difficult to grow cracks stably and obtain data at ambient temperature due to the brittle nature of the material. Fatigue cracks were grown in single edge notched specimens having a gauge section 20 mm wide and approximately 3 mm thick. The notch, made using a low speed diamond saw, was approximately 0.5 mm wide and 3 mm deep. Cracks were initiated by compression-compression loading at an equivalent $\Delta K = 30 \text{ MPa}\sqrt{\text{m}}$. After initiation and some growth, cycling was changed to tension-tension loading at

$R = 0.1$ ($R = \text{minimum/maximum stress intensity}$) at 1 Hz. Most of the cyclic loading was applied in a laboratory fatigue machine in a vacuum of $\approx 10^{-5}$ torr. The temperature of test was achieved by radiant heating from a resistance heated furnace within the vacuum chamber and was measured with a thermocouple attached to the specimen gauge section.

Specimens were periodically cooled and transferred from the laboratory machine to a special hydraulic cyclic loading frame fitted with a resistance heating furnace which fit within the scanning electron microscope. Crack growth was thus observed with the high resolution and large depth of field conditions available with the SEM while, at the same conditions of loading and temperature used in the laboratory machine. By working in vacuum, environmental effects on crack growth were largely excluded.

Results

Measured fatigue crack growth rates at ambient and 800°C are shown in Fig. 11. The ambient temperature value shown at 10^{-10} m/cy was laboriously derived and is the best value of ΔK_{th} which could be determined. During the experiment to obtain ΔK_{th} , the crack would not grow for many thousands of cycles at the ΔK being applied, and then would then grow suddenly on one side of the specimen, but not on the other. The erratic growth characteristics and low fracture toughness of this material made the task of measuring crack tip parameters at ambient temperatures so difficult that few have been obtained to date.

A sequence of photographs showing the growth of a crack through the material at 800°C is shown in Fig. 12. The crack growth sequence begins with the crack in equiaxed grains of γ , then crosses the boundary from this microstructure to the lamellar $\alpha_2 + \gamma$ region. The orientation of the lamellae relative to the direction of crack growth was such that the crack grew parallel to the lath boundaries for a considerable distance. Subsequent increase of the stress intensity level did not alter the direction of growth. Careful examination of these photographs does not indicate that a slip line is forming at the crack tip; however, the crack tip does undergo a bit of blunting before it increases in length. This blunting and sharpening in connection with crack growth has been observed in other alloys frequently, and it was seen also for fatigue crack growth in partially stabilized zirconia. The absence of

slip line formation for this material makes it different from the other titanium alloys studied thus far.

For the sequence shown in Fig. 12, the relationship between crack length and number of cycles, and the accompanying average crack growth rates are shown in Fig. 13. These results indicate that the crack growth rate is approximately constant in the equiaxed structure, increase as the crack traverses the boundary between equiaxed and lamellar microstructures, and decreases as it grows within the lamellar region.

Measurements of crack opening displacements and displacements within the region influenced by the crack tip were measured from photographs of the crack tip made in the SEM cyclic stage at 800°C. Photographs made at minimum and maximum load were compared using stereomaging and displacements were measured with the DISMAP image processing system. As for fatigue cracks in many other materials, the Mode I crack opening displacement (COD I) was related to the distance behind the crack tip (d) by

$$\text{COD I} = C_o \sqrt{d} \quad (10)$$

where C_o is a constant. The gradients of the displacements were computed to determine the three elements of the in-plane strain tensor, from which the effective strain and the principal strains were computed.

The distributions of strain parallel (x -direction) and perpendicular (y -direction) to the loading axis were determined and found to fit the function,

$$\varepsilon'(r) = A' - m \ln(B+r) \quad (11)$$

where $\varepsilon'(r)$ = (strain at the distance r /strain at the crack tip) better than a power function [$\varepsilon'(r) = A'/(b+r)^m$], just has been found for a number of other alloys. Values derived for the constants in eq. (11) from 14 sets of data are:

$$\begin{aligned} 1.10 < A' < 1.30 \\ B &= 2 \\ 0.280 < m' < 0.434 \end{aligned}$$

for the range $14 < \Delta K \leq 22 \text{ MPa}\sqrt{\text{m}}$.

Values of the constants for each analysis of crack tip strain, together for crack tip strain, $\epsilon'(r)$, are listed in Table 3, together with other derived constants.

Table 3
Crack Tip Parameters

ΔK MPa \sqrt{m}	$\Delta\epsilon(0)$	Dir'n.	B μm	m'	A'	PZS μm	C_0 μm	U
14.2	0.0824	x	2	0.280	1.194	59.5	0.44	0.63
		y	1	0.217	1.00	82.2		
14.2	0.0944	x	2	0.291	1.202	53.1	0.51	
		y	2	0.161	1.111	79.5		
17.1	0.20	x	2	0.361	1.250	28.5	0.90	
		y	2	0.310	1.215	45.7		
17.1	0.065	x	2	0.307	1.213	42.0	0.63	0.50
		y	2	0.307	1.213	42.0		
17.2	0.059	x	2	0.434	1.300	15.6	0.38	
		y	2	0.279	1.193	56.7		
17.2	0.071	x	2	0.281	1.195	57.5	0.071	
		y	2	0.281	1.195	57.5		
21.6	0.129	x	2	0.323	1.224	38.8	0.55	
		y	2	0.280	1.194	62.8		
28.4	0.130	x	2	0.154	1.11	1216 *	2.44	
		y	2	0.187	1.13	391		
56.8	0.513	x	2	0.167	1.116	781	5.65	
		y	2	0.169	1.117	726		

* intense shear band formed approximately parallel to loading axis.

Two direct measurements of the load needed to open the crack to the tip in Mode I were also made. These measurements of closure were made as explained in the section A. Opening load was used to compute U , as previously defined, and it is graphed vs $1/K_{\max}$ in Fig. 14. There is some uncertainty in the measured values of opening load, and these are shown in the figure. The scatter makes it difficult from these data alone to estimate ΔK_{th} - the value is $6.6 \pm 1.5 \text{ MPa}\sqrt{\text{m}}$ - but this helps define the value of crack growth rate at 10^{-10} m/cy shown in Fig. 11. Knowing ΔK_{th} , it is, therefore, possible to determine ΔK_{eff} , and this has been used in subsequent analyses.

Plastic zone sizes given in the Table were computed from the strain distributions to a point where the (cyclic) strain was twice the elastic value (0.0033); thus, the dimension given should be considered the cyclic plastic zone size.

The relationships between C_o (which may also be defined as the CTOD) and $\Delta\varepsilon(0)$ (the crack tip strain) and ΔK_{eff} are shown in Fig. 15. The slopes of these relationships are effected by the values at large ΔK , and there is considerable scatter in the values when measurement is repeated, as it was at $\Delta K \approx 17 \text{ MPa}\sqrt{\text{m}}$. Least squares fit to the data of Fig. 15 give

$$\text{CTOD} = 0.03 \Delta K_{eff}^{1.26} \quad (12)$$

$$\Delta\varepsilon(0) = 0.016 \Delta K_{eff}^{0.77} \quad (13)$$

and these may be combined to give a relation between $\Delta\varepsilon(0)$ and CTOD

$$\Delta\varepsilon(0) = 0.137 \text{CTOD}^{0.61} \quad (14)$$

This function fits the data overall, but as may be seen in Fig. 16, there emerges a different relationship for the data taken at low ΔK . If only these data are considered, the slope of eq. (14) becomes ≈ 2 .

Discussion

Further investigation of fatigue crack growth through $\alpha_2+\gamma \text{ TiAl}$ remains to be accomplished, particularly for cracks growing across the lamellar plates

at 800°C, if that can be induced. Also, further work remains to be done at ambient temperature where the material shows much less capacity for deformation and crack growth is much less stable.

A comparative analysis should be made between this titanium aluminide and other alloys based on α_2 (Super α_2 and 2411). This analysis, together with previous work, would then bridge the phases in the titanium system: $\alpha+\beta+\alpha_2+\gamma$. From this systematic analysis, an understanding of the relationship between microstructure and crack tip micromechanics will be sought. However, this study will be complicated by the lamellar microstructures of the $\alpha_2+\gamma$ TiAl alloys, and it may be necessary to also study fatigue crack growth through a lower toughness equiaxed microstructure.

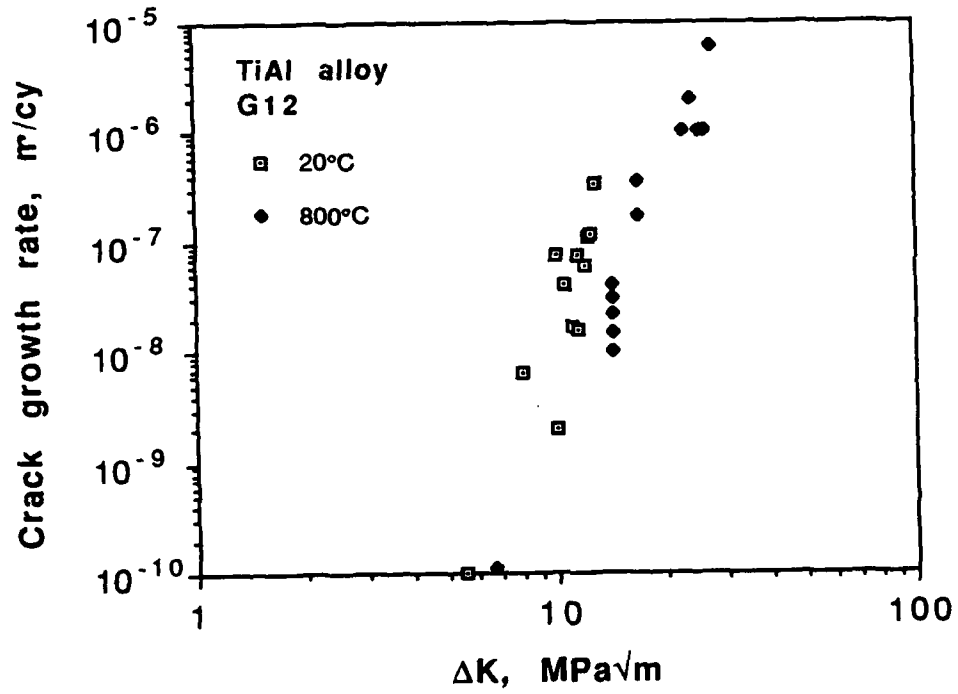


Fig. 11 Fatigue crack growth rates for the TiAl alloy at ambient and 800°C.

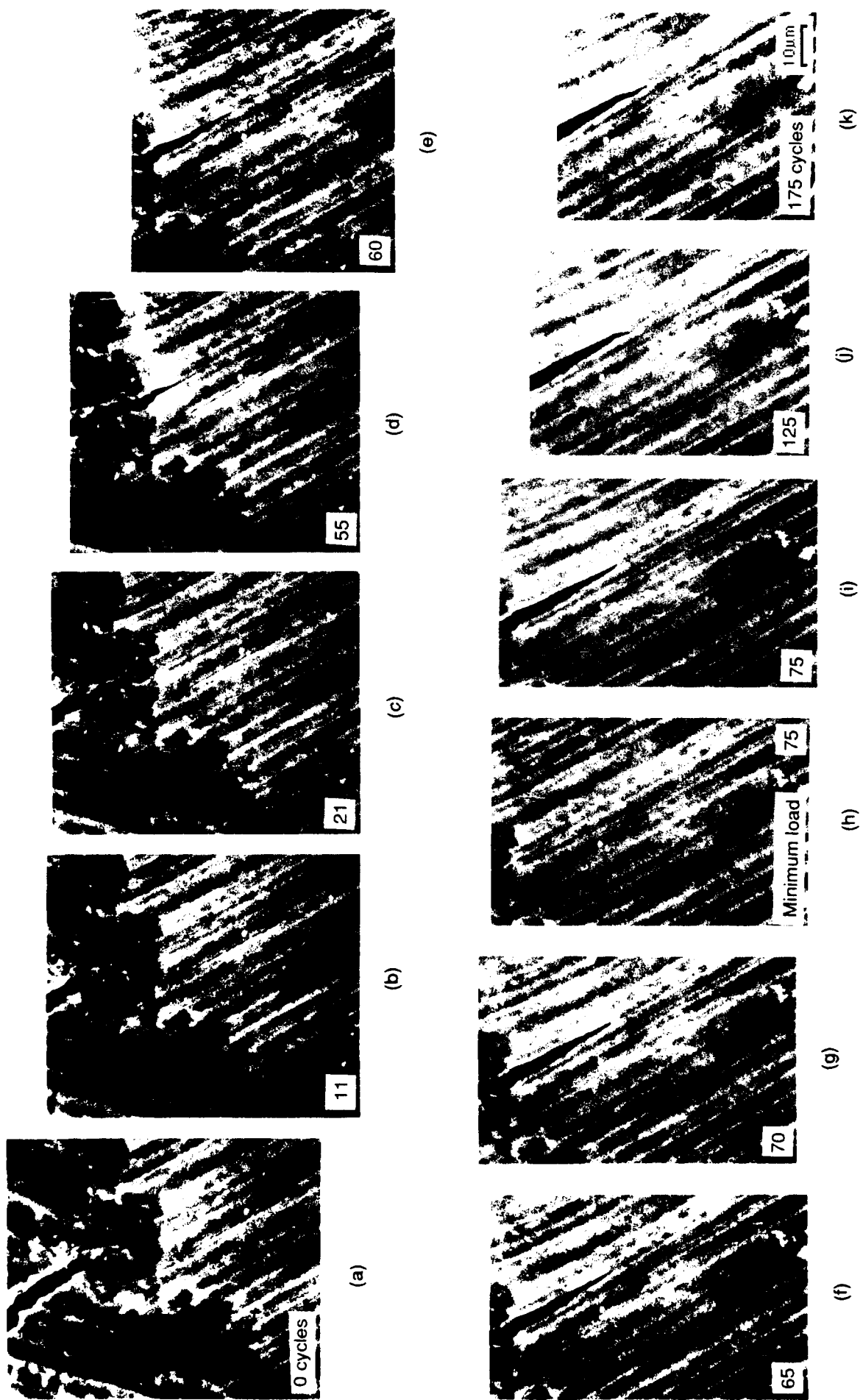


Fig. 12 Photographs of the crack tip showing the growth of a fatigue crack in TiAl alloy at 800°C, $\Delta K = 17 \text{ MPa}\sqrt{\text{m}}$. Sequence starts in (a) at 0 cycles, and the number of cycles for each of the subsequent photographs is shown in the lower left of the figure. Note how tightly the crack is closed at minimum load, as shown in (h).

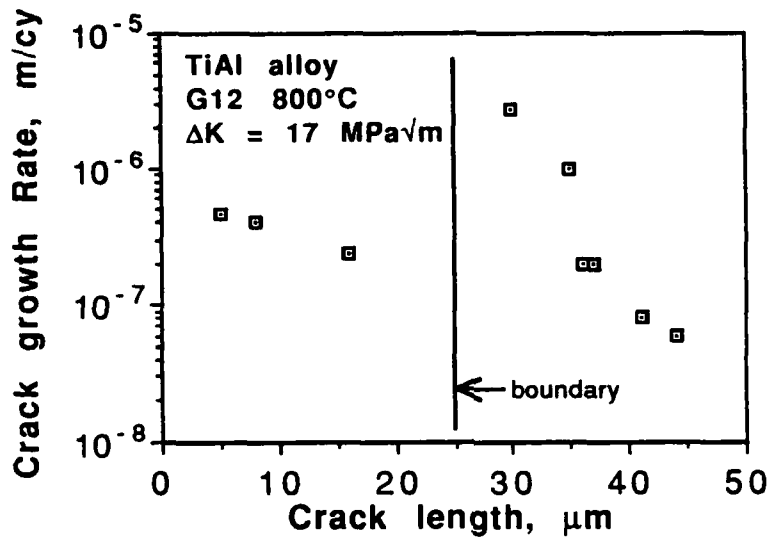
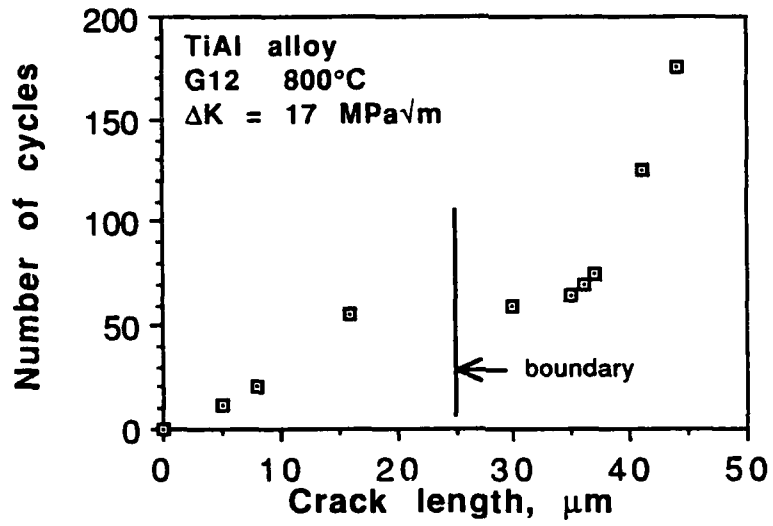


Fig. 13 (a) Crack length vs number of cycles and (b) crack growth rate vs crack length for the crack growth shown in Fig. 12.

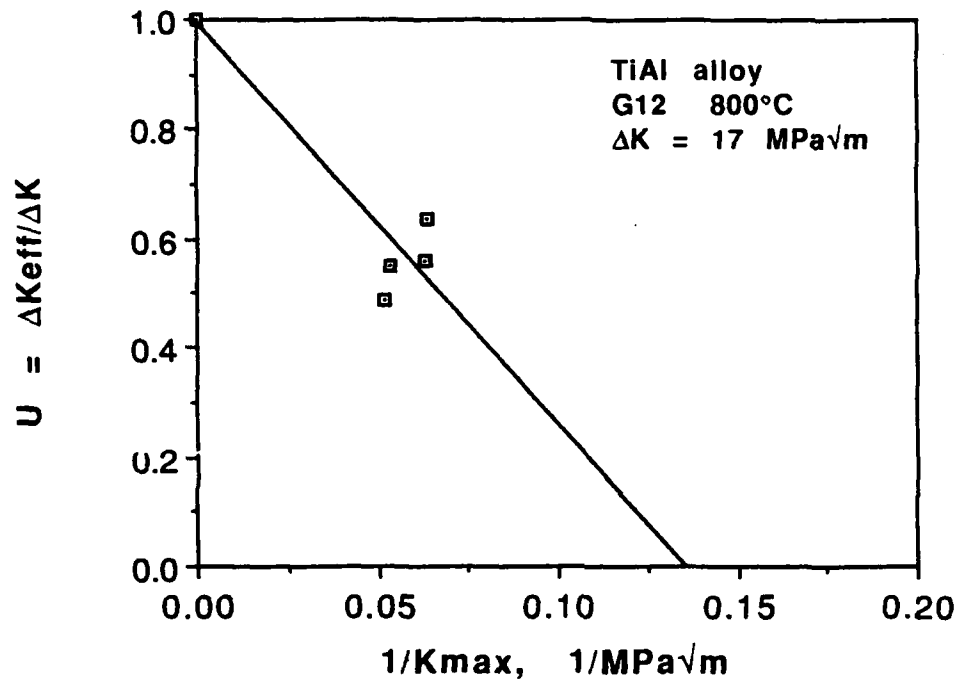


Fig. 14 Fatigue crack closure measurements for TiAl alloy at 800°C.

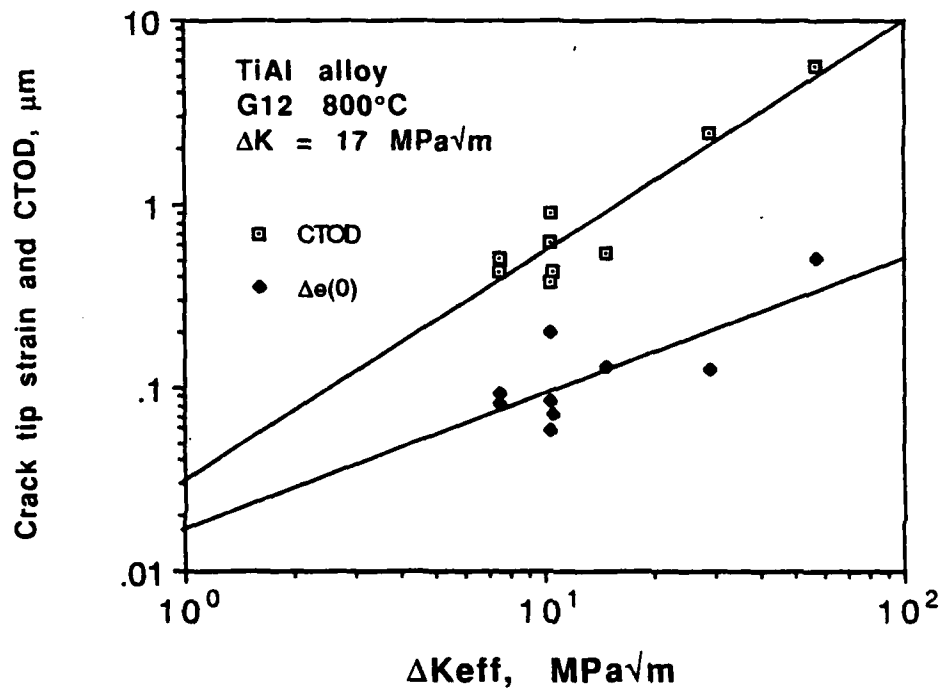


Fig. 15 Crack tip opening displacement (CTOD) and crack tip strain vs ΔK_{eff} for fatigue cracks grown in the TiAl alloy at 800°C.

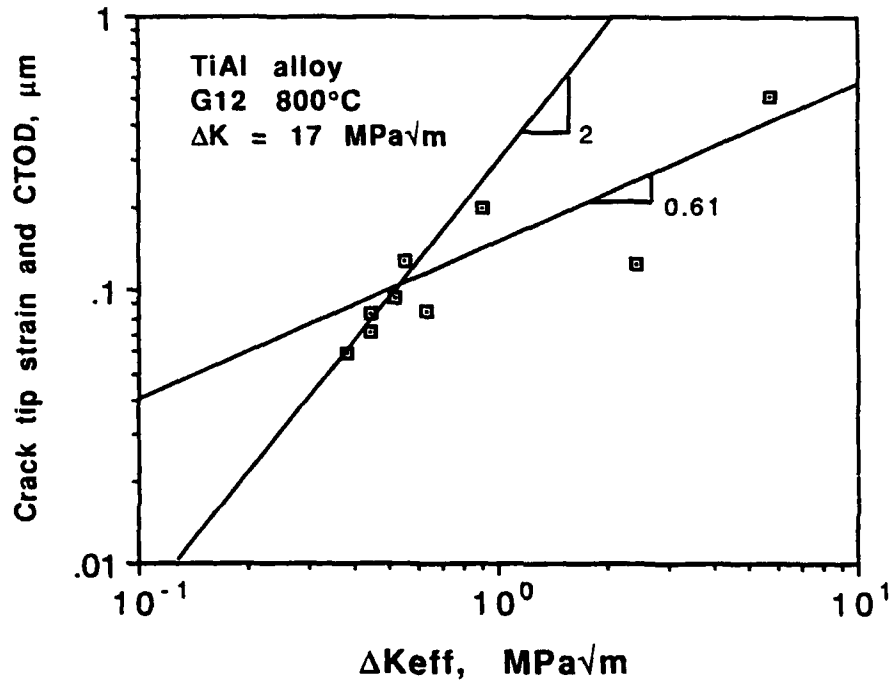


Fig. 16 Crack tip strain vs CTOD for fatigue cracks grown in the TiAl alloy at 800°C.

IV. FRACTURE TOUGHNESS

The influence of microstructure on the fracture and toughening processes in two classes of two-phase titanium aluminide alloys was studied during the last reporting period. The alloys studied included: (1) an $\alpha_2 + \beta$ alloy, which was Ti-24Al-11Nb; and (2) a near gamma alloy, which was Ti-47Al-2.6Nb-2(Cr + V). The Ti-24-11 alloy was purchased from TIMET, while the Ti-47Al-2.6Nb-2(Cr + V) alloy was supplied by Metcut-Material Research Group at Wright-Patterson AFB (WPAFB) through Dr. Y.-W. Kim. The emphasis of the work performed last year was focused on the two-phase gamma alloy.

The roles of microstructure in the fracture toughness and tensile ductility of the two-phase titanium aluminide alloys were established by identifying the relevant fracture and toughening processes in these alloys by performing crack-tip micromechanics experiments both at ambient and elevated temperatures. Additionally, strain distribution within the crack-tip plastic zone was measured using the machine-vision-based stereoimaging technique developed at SwRI. The in-situ observations of the near-tip fracture processes and strain measurements were used in conjunction with micromechanical modeling to distinguish the various roles of the ductile phase in the fracture and toughening mechanisms, and to establish microstructure/toughness relationships in these representative two-phase titanium aluminide alloys. Most of these results are reported in four separate papers [34-37], with a fifth in preparation. Key findings of these research activities are highlighted in the following sections:

A. Microstructure/Toughness Relationships in Two-Phase ($\alpha_2 + \beta$) Titanium Aluminide Alloys

The toughening mechanisms in Ti-24Al-11Nb were previously identified [38] to include crack-tip blunting, crack deflection, and crack bridging, all of which were contributed at least partly, if not totally, by the ductile, disordered, body-centered cubic β phase. These fracture and toughening characteristics, which are typical of alpha-two titanium aluminide alloys, indicated that fracture toughness in the Ti-24-11 alloy originated from both intrinsic and extrinsic means. Intrinsic mechanisms, which include crack-tip blunting by a ductile phase, are expected to influence the initiation toughness (i.e., K_{IC}) values. In contrast, extrinsic mechanisms, which include microcrack shielding, crack deflection, and crack bridging by a ductile phase, are expected to affect the crack growth toughness and lead to a resistance-curve behavior.

To study the influence of the morphology and volume fraction of the ductile beta phase on the fracture mechanisms and the associated toughness responses, critical in-situ fracture experiments were performed on the Ti-24-11 alloy heat-treated to contain either a coarse basketweave or a fine basketweave microstructure, whose fracture behaviors were then compared with those for the equiaxed microstructure, which was studied earlier in this program [34]. Micrographs showing these three microstructures are presented in Fig. 17. Relevant information of the microstructure including the volume fraction of the beta phase and the size of the α_2 grains were measured, and the results are summarized in Table IV, together with the tensile and fracture properties. The J-resistance curves for the equiaxed, coarse basketweave, and fine basketweave microstructures at ambient temperature are compared in Fig. 18. The comparison indicated that microstructure exerted a significant influence on both the initiation and crack growth toughness values of the Ti-24-11 alloy at ambient temperature. In contrast, the J-resistance curves for 600°C, which showed exceptional crack growth toughness, were found to be relatively insensitive to microstructure, as shown in Fig. 19.

The differences in the fracture processes in the equiaxed, coarse and fine basketweave microstructures at the ambient temperature were found to arise from two sources: (1) volume fraction of the beta phase, and (2) the continuity of the beta phase. The importance of these two aspects the microstructure is illustrated in Figs. 20 and 21, which show the interaction of the crack tip with the microstructure in the coarse and fine basketweave materials, respectively. Fig. 20 shows that both the main crack and microcracks in the coarse basketweave microstructure, which contained 39 vol. % of the continuous β phase, were blunted by the continuous beta phase, resulting in relatively large crack opening displacements and a K_{IC} value of $21.5 \text{ MPa}\sqrt{m}$. In contrast, the main crack in the fine basketweave material, which contained 25 vol. % of the beta phase in discontinuous forms, was seen to propagate around and through the smaller, discontinuous beta phase, Fig. 21. The lack of involvement by some of the discontinuous beta phase in the fracture process led to a relatively low K_{IC} value ($15 \text{ MPa}\sqrt{m}$) and no tearing resistance.

The relative contributions of various toughening mechanisms to the overall toughness in the three microstructures of the Ti-24-11 alloy were distinguished by theoretical calculations, using relevant micromechanical models described in the literature or formulated in this program. The micromechanical models considered included those of microcrack shielding [39], crack deflection [40], and crack bridging by a ductile phase [41]. A micromechanical model which considered toughness enhancement resulting from blunting of the crack tip by a ductile ligament does not exist in the literature. A simple model of this type was therefore formulated in this

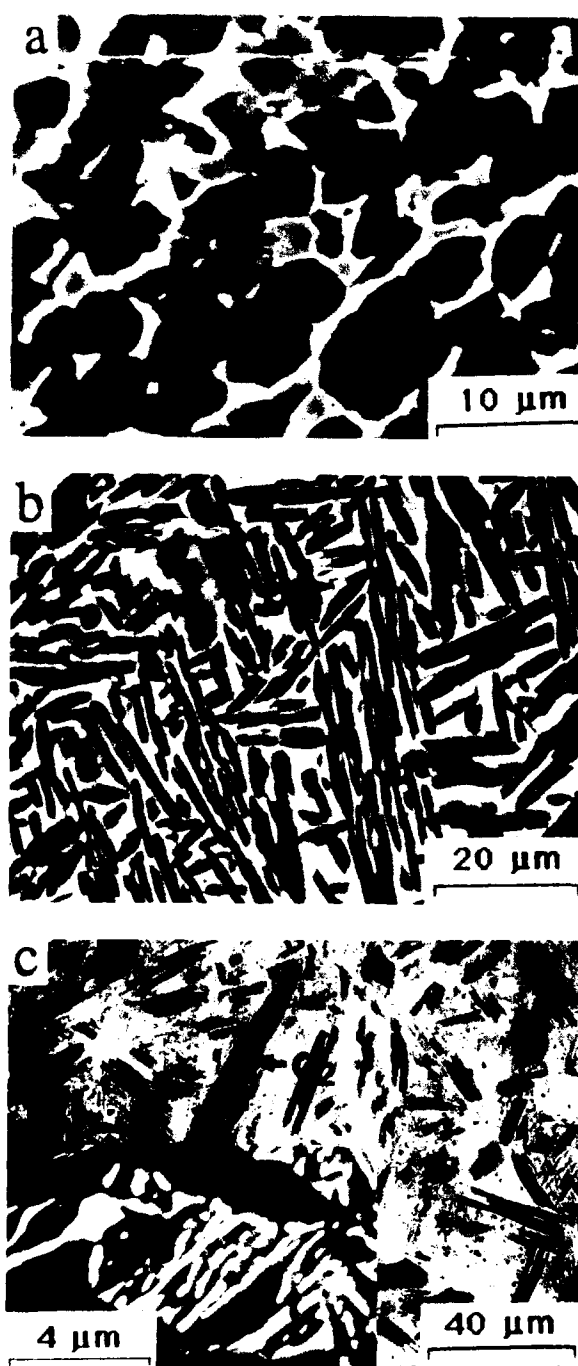


Fig. 17 Typical equiaxed (a), coarse basketweave (b), and fine basketweave (c) microstructures.

Table 4. Summary of Tensile, Fracture, and Microstructural Properties of Ti-24Al-11Nb

Microstructure	T, °C	Yield Stress, MPa	Ultimate Tensile Strength, MPa	Young's Modulus, MPa	Strain Hardening Exponent	Total Elongation, %	Fracture Strain, %	K_{IC} , MPa \sqrt{m}	Tearing Modulus, T_R	Vol. Fraction of β , %	α_2 grain size, μm
Equiaxed $\alpha_2 + \beta$	25	648.8	692.9	9.38×10^4	0.053	2.11	4.2	20.4	1.5	26	6.8
	600	378.8	636.5	5.3×10^4	0.133 0.357	38.8	64.1	12.5	90.0		
Coarse Basketweave	25	461.9	688.7	9.0×10^4	0.120	3.8	4.0	22.5	0	39	4.0
	600	344.9	681.6	6.0×10^4	0.124 0.304	20.0	29.5	18.2	49.2* 95.9		
Fine Basketweave	25	688.4	842.6	7.7×10^4	0.09	3.1	3.2	15.0	0	25	4.5 (primary α_2)
	600	442.1	767.8	7.6×10^4	0.138 0.394	24.4	35.1	19.8	73.4* 88.0		

* Based on the initial slope of the J vs Δa curve.

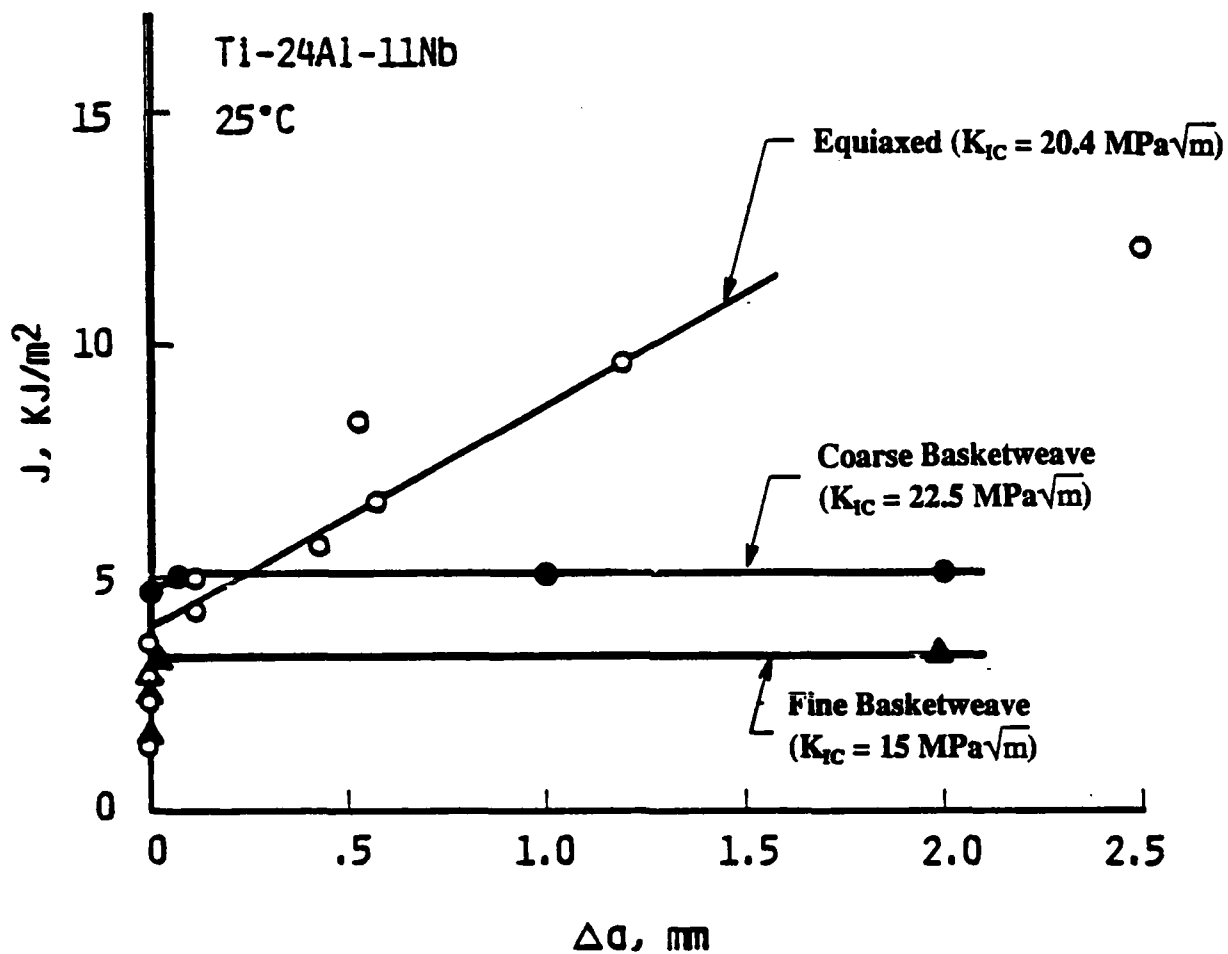


Fig. 18 Comparison of J-resistance curves for the equiaxed, coarse basketweave, and fine basketweave microstructures of the Ti-24Al-11Nb alloy at 25°C.

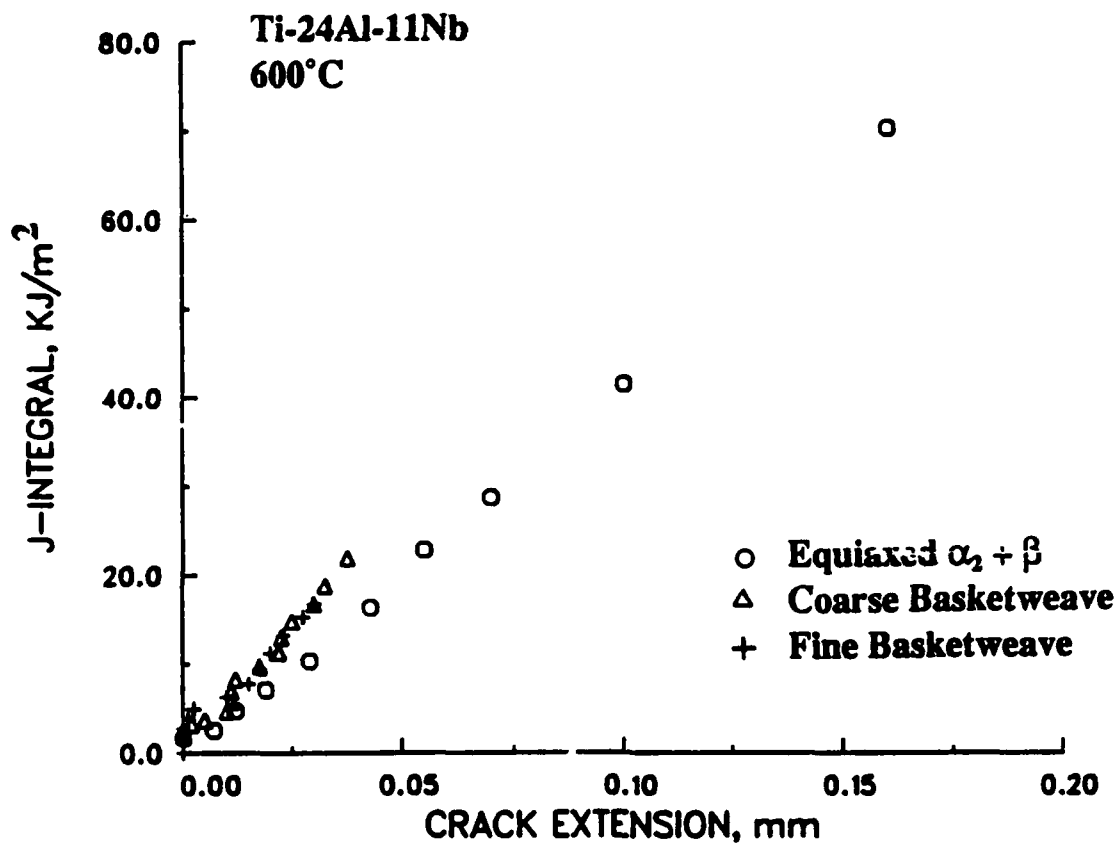


Fig. 19 Comparison of J-resistance curves for the equiaxed, coarse basketweave, and fine basketweave microstructures of the Ti-24Al-11Nb alloy at 600°C.

Ti-24Al-11Nb
Coarse Basketweave Microstructure
25°C

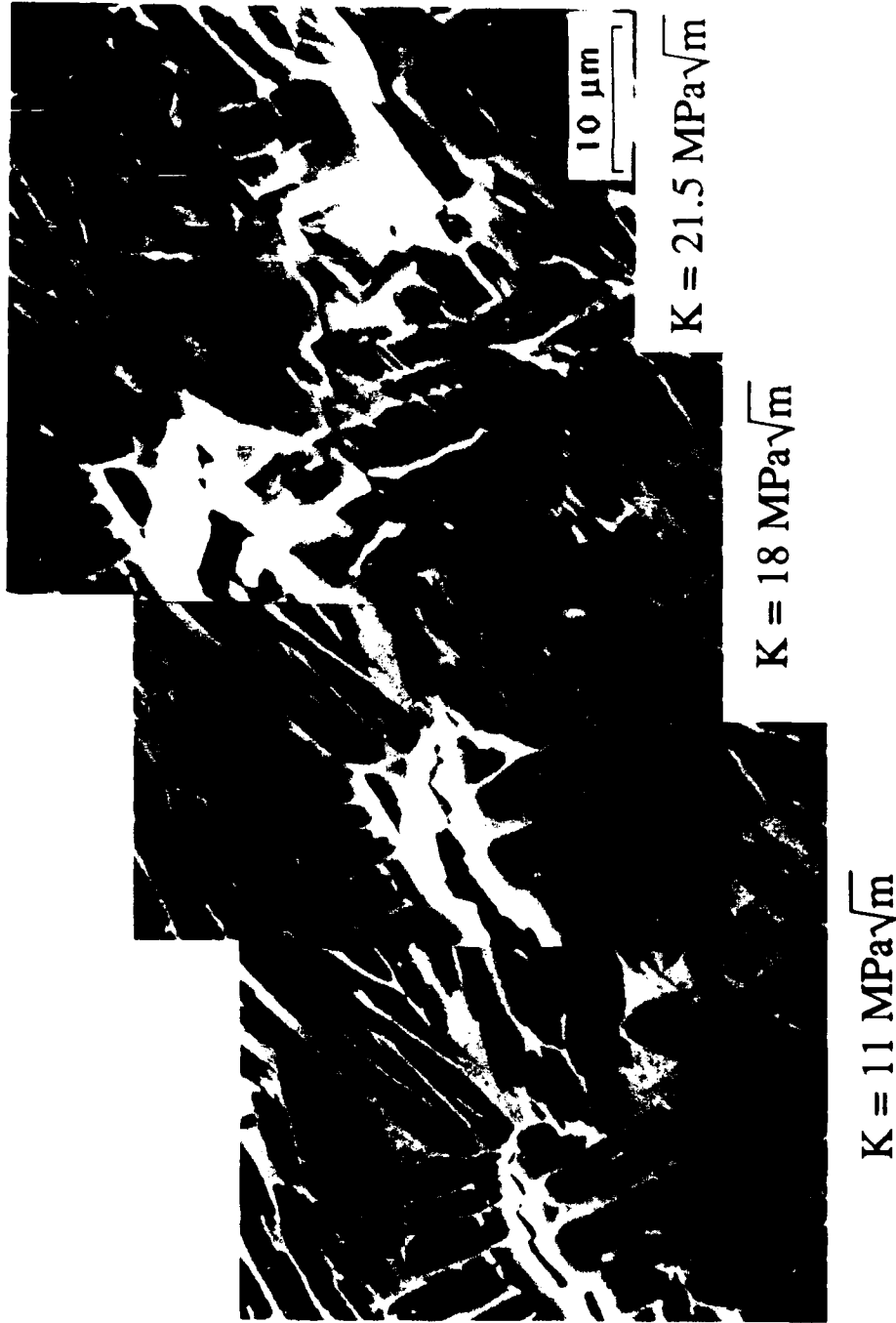


Fig. 20 Composite in-situ SEM micrographs showing the near-tip fracture process in the coarse basketweave microstructure is characterized by blunting of the tips of the main crack and microcracks by the continuous β phase. The volume of β is 39%.

Ti-24Al-11Nb
Fine Basketweave Microstructure
25°C

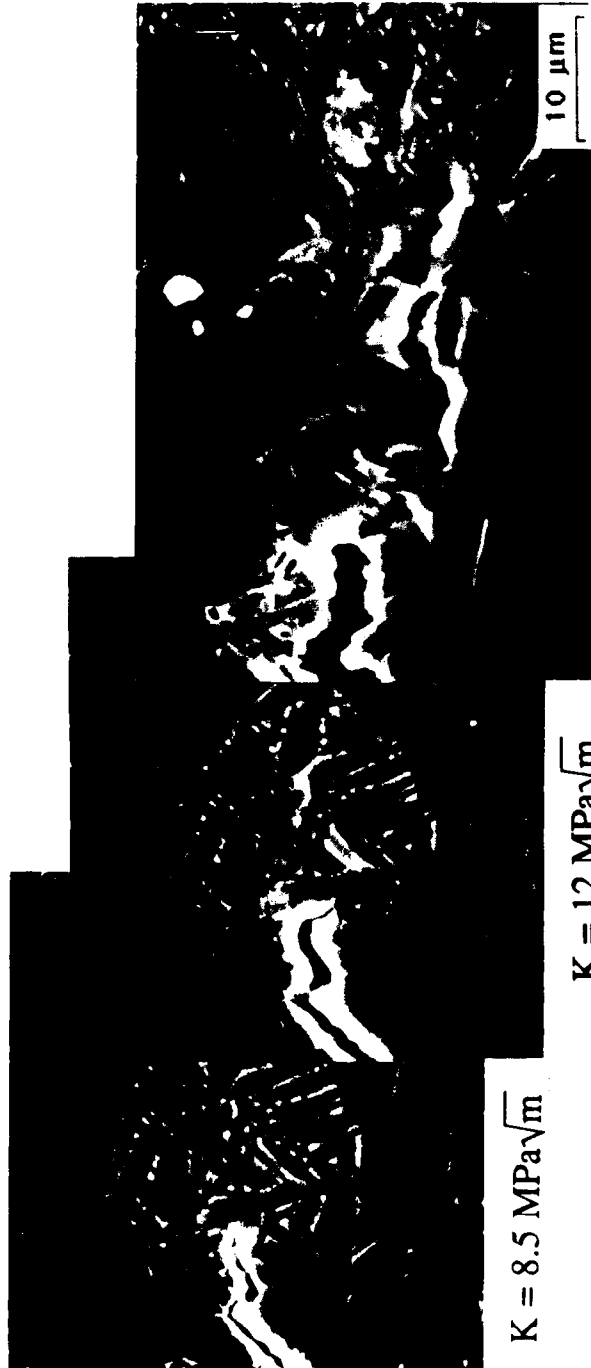


Fig. 21 Composite in-situ SEM micrographs showing the near-tip fracture process in the fine basketweave microstructure is characterized by propagation of the main crack around and through the smaller, discontinuous β phase. The volume fraction of β is 25%.

program [34]. These various micromechanical models were used to compute individual values of the toughening ratio, a measure of toughness enhancement, for a given toughening mechanism. Details of these micromechanical calculations and results were presented in [34]. As described in [34], the toughening ratio was defined as the ratio of the resultant toughness when a particular toughening mechanism was operative to the matrix toughness. Comparison of the observed and calculated toughening ratios for crack deflection (λ_d), microcrack shielding (λ_m), and ductile phase blunting (λ_b), as well as those for all of the shielding mechanisms (λ_s) and the overall toughening ratio (λ) revealed that crack-tip blunting by the ductile phase was the dominant toughening mechanism in the Ti-24-11 alloy at 25°C [34]. **Fig. 22** compares the crack-tip blunting model with the experimental K_{IC} results from this study [34,38] and other previous investigations [42-44]. Both positive and negative deviations from the crack-tip blunting model were observed in **Fig. 22**. Positive deviations were attributed to the presence of toughening mechanisms other than crack-tip blunting, while negative deviations were found to be associated with the ineffectiveness of the discontinuous beta phase in the crack-tip blunting process [34].

Based on both experimental and analytical results, it was concluded that the initiation toughness (K_{IC}) of the Ti-24-11 alloy at 25°C originated from crack-tip blunting by the ductile phase, the matrix toughness, and, to a lesser extent, crack deflection. The crack growth toughness in the equiaxed microstructure at 25°C was found to originate from ductile phase bridging and toughening by shear ligaments [37] which were formed as the results of mismatched planes of microcracks and the main crack. At 600°C, the ductile beta phase appeared to play an insignificant role in the toughening process. The exceptional crack growth toughness observed in the equiaxed, coarse basketweave, and fine basketweave microstructure appeared to arise from crack-tip plasticity, which was dominated by the matrix phase. In the latter two microstructures, the crack growth toughness was also enhanced by the formation of a profuse zone of microcracks at the crack wake after crack extension had occurred [34].

B. Microstructure/Toughness Relationships In Two-Phase Gamma Titanium Aluminide Alloys

The roles of microstructure in the fracture and toughening processes in two-phase gamma titanium aluminide were examined by studying two contrasting microstructures of the Ti-47Al-2.6Nb-2(Cr + V) alloy. The microstructures were: (1) an predominantly equiaxed γ grain microstructure with small amounts of α_2 particles

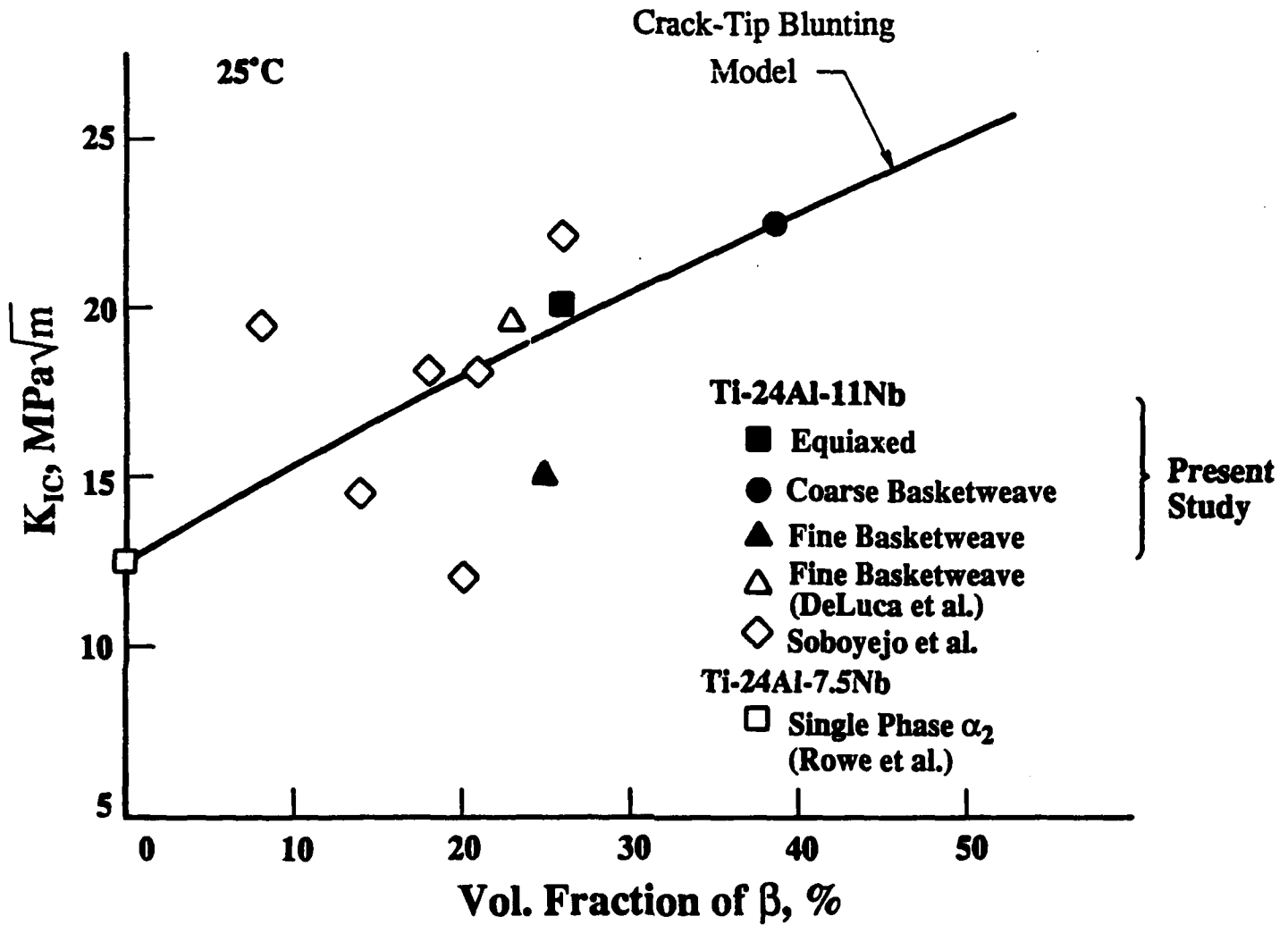


Fig. 22 Comparison of calculated initiation toughness (K_{IC}) with measured values from this study and those from Soboyejo et al. [25] and DeLuca et al. [26]. The result of Rowe et al. [27] for single phase α_2 Ti-24Al-7.5Nb alloy was used as an input to the crack-tip blunting model.

Table 5. Heat-Treatment Procedures, Microstructures, Tensile, and Fracture Properties of the Near Gamma Alloy, Ti-47Al-2.6Nb-2(Cr + V).

Material*	Heat-Treatment	Microstructure	T, °C	σ_y , MPa	σ_{UTS} , MPa	Total Elongation, %	K_{IC} , MPa \sqrt{m}	T_R	K_S , MPa \sqrt{m}
G1F	1275°C/3 hrs in vacuum/ controlled cool to 900°C. Aging at 900°C/4 hrs/FC in vacuum.	Predominantly equiaxed γ plus small amounts of α_2 particles and plates.	25	415.6	557.9	3.7	11.4	0	11.4
			600	342.0	600.5	7.3	16.1	0	16.1
			790	168.4	295.9	13.0	--	--	--
G1L	1360°C/1 hr in vacuum/ controlled cool to 900°C. Aging at 900°C/6 hrs/AC	Predominantly lamellar α_2 + γ microstructure plus small amounts of equiaxed γ grains at colony boundaries.	800	289.4	377.6	1.50	35.0	102.0	>61.0
			25	329.6	383.1	0.88	16.0	0.94	25.0

* Asymptotic or maximum value of stress intensity factor in the K-resistance curve.

+ Materials supplied by Metcut-Material Research Group at Wright-Patterson AFB.

and plates (G1F), and (2) a predominantly lamellar $\alpha_2 + \gamma$ microstructure with small amounts of equiaxed γ grains at lamellar colony boundaries (G1L). Micrographs showing these two contrasting microstructures are presented in **Fig. 23**.

Both conventional and in-situ tensile and fracture tests were performed at selected temperatures ranging from 25 to 800°C. Most of the experiments were, however, conducted in a SEM equipped with a high-temperature loading stage to allow for in-situ observations of the fracture processes and the interactions of the crack tip with relevant microstructural features. Selected tests were repeated in air using conventional testing techniques to examine possible environmental effects both at ambient and elevated temperatures (e.g., at 800°C). No evidence of environmental effects was found at 25°C, but some evidence was observed at 800°C. Summary of the tensile ductility and fracture toughness values for the two microstructures of the Ti-47Al-2.6Nb-2(Cr + V) alloy is presented in Table V. As shown in Table V, the equiaxed γ grain microstructure (G1F) was found to exhibit higher tensile ductility, but lower fracture toughness values than the lamellar microstructure (G1L) at both ambient and elevated temperatures. Comparison of the K-resistance curves of the two microstructures for various temperatures, **Fig. 24**, revealed that the lamellar microstructure exhibited higher initiation and crack growth toughness over the range of temperatures examined.

The fracture processes in the G1F and G1L microstructures were identified by in-situ observations in the SEM. The dominant fracture mechanisms in the equiaxed γ (G1F) microstructure were grain boundary decohesion, **Fig. 25(a)**, and quasi-cleavage fracture along localized slip bands in γ grains. In contrast, fracture mechanisms in the G1L microstructure involved crack deflection at the α_2/γ interface, microcrack formation ahead of the deflected crack tip, and shear fracture of ligaments located between the main crack and the microcracks, **Fig. 25(b)**. The possibility of additional toughening effects originated from fracture of the shear ligaments, which were formed in the process zone as the consequence of crack deflection and mismatched planes of the main crack and microcracks, was examined by micromechanical modeling [37]. The analytical results indicated that shear ligament toughening could arise from plastic, and possibly frictional, dissipation associated with the fracture of shear ligaments in the crack-tip process zone [37]. This occurred when the energy dissipation associated with fracture of the shear ligaments exceeded those for matrix cracking. Another possible source of toughness in the lamellar microstructure was the ductility of α_2 platelets. Near-tip strain distribution obtained at $K = K_{IC}$ revealed that the lamellar microstructure was able to sustain higher crack-tip strains than the equiaxed gamma microstructure, as shown in **Fig. 26**.

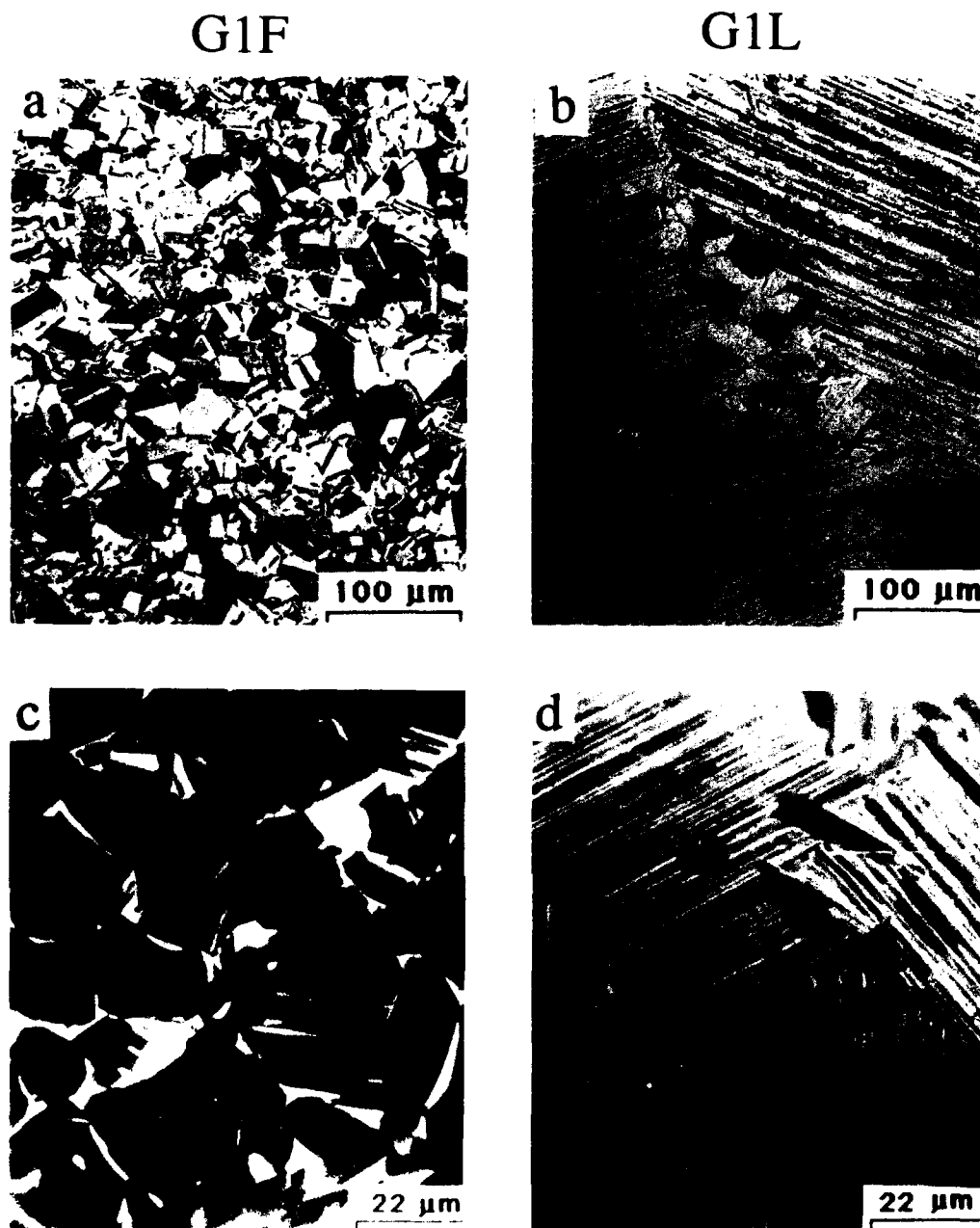


Fig. 23 Microstructures of G1F (a, c) and G1L (b, d) showing: fine gamma grains in optical micrograph (a) with grain boundary alpha-2 phases imaged bright in the back-scattered electron image (c); large lamellar grains (b) consisting of alternative layers of gamma plates and alpha-2 plates (d) with fine grain boundary gamma. The alpha-2 plates in the lamellar structure are imaged light in the back-scattered electron image (d).

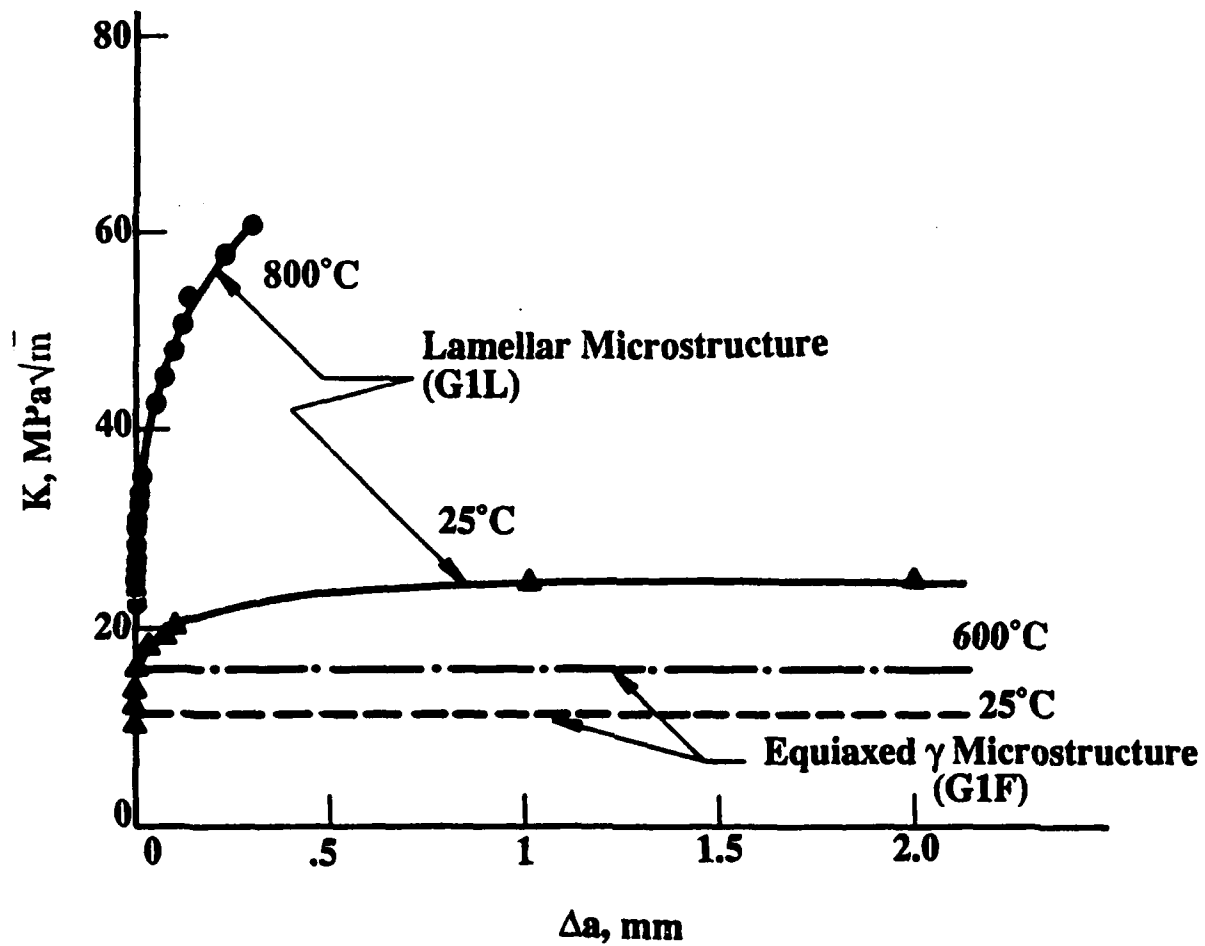
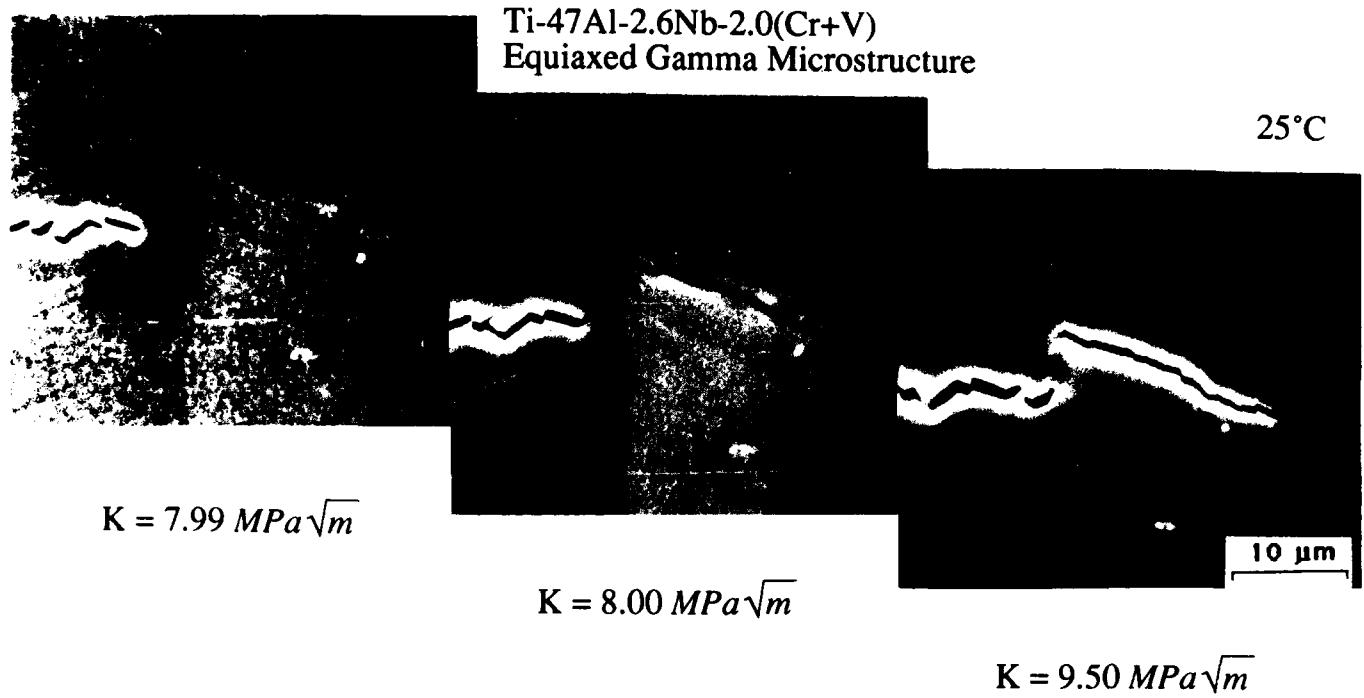
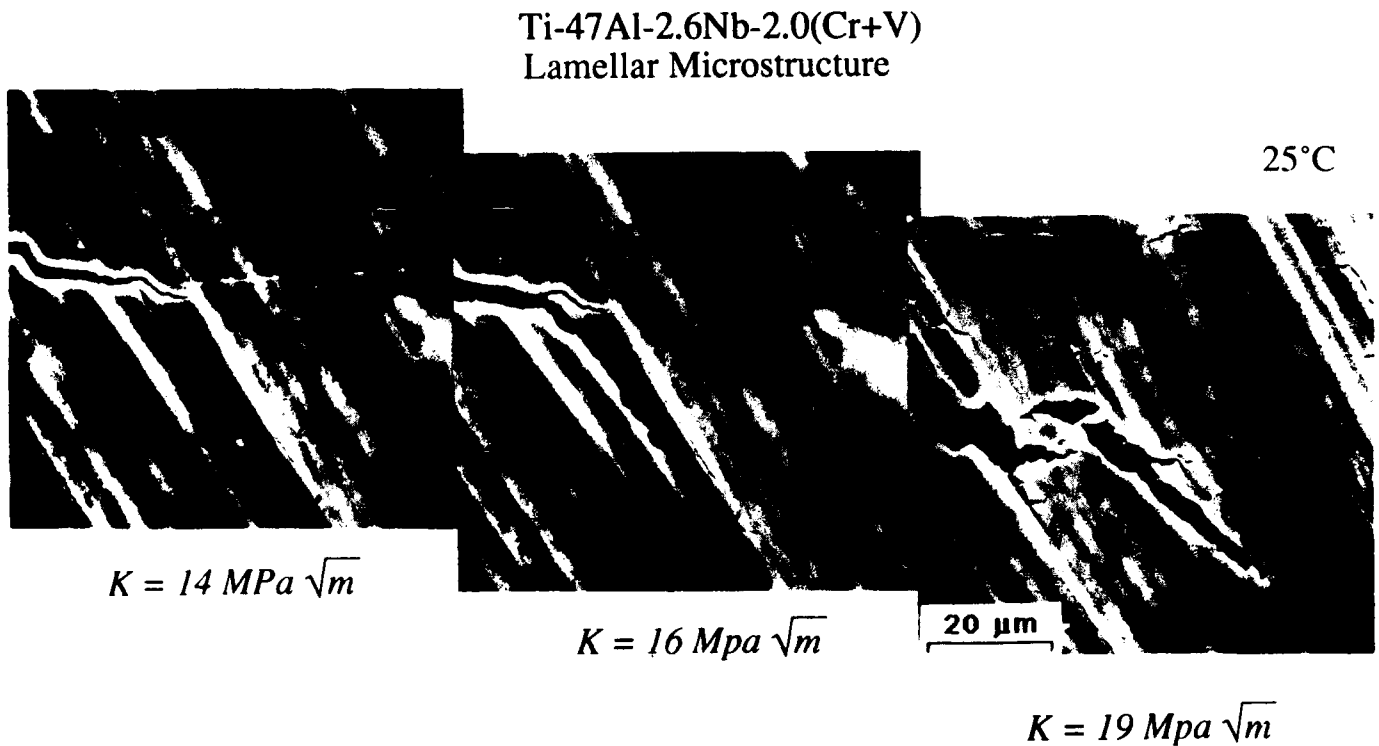


Fig. 24 Comparison of the K -resistance curves for the lamellar microstructure at various test temperatures. The lamellar microstructure exhibits higher K_{Ic} values and crack growth resistance both at ambient elevated temperatures, when compared to the equiaxed γ microstructure.



(a) Fracture by grain boundary decohesion in the equiaxed γ microstructure.



(b) Fracture by translamellar and apparent interface propagation with microcrack formation in the lamellar microstructure.

Fig. 25 Composite in-situ SEM micrographs showing the near-tip fracture process in the Ti-47Al-2.6Nb-2(Cr + V) alloy.

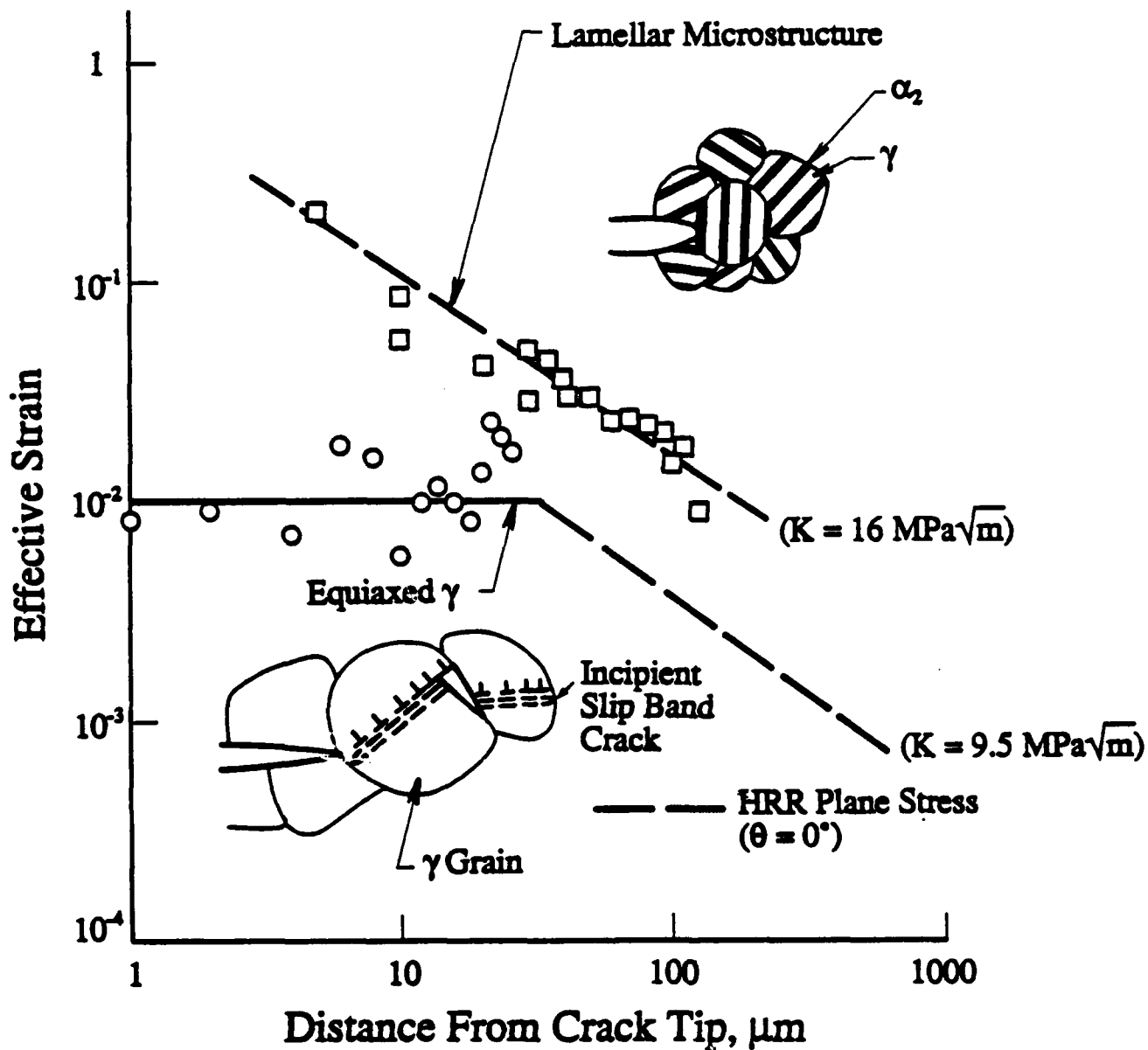


Fig. 26 Near-tip effective strain measurements showing higher strain values in the lamellar microstructure than in the equiaxed γ microstructure.

In spite of lower fracture toughness, the equiaxed γ microstructure exhibited a higher tensile ductility. The higher tensile ductility observed in this microstructure was found to be a crack size effect, which manifested as a grain size effect. This phenomenon arose because of the propensity of the gamma alloy for nucleation of microcracks. Once nucleated, propagation of the microcracks to final fracture would be controlled the toughness of the materials. Microcracks in the G1F microstructure were grain boundary microcracks or slip band cracks on the order of the grain size, which was approximately 40 μm in diameter. In contrast, the microcracks in the lamellar microstructure, which occurred by delamination of the α_2/γ interface, were on the order of the colony size, typically about 1.6 mm in diameter. This particular K_{Ic} -controlled fracture process in a tensile specimen was modeled to investigate possible relationships between K_{Ic} , grain (or crack) size, and tensile ductility [35]. Detailed description of the model was presented in [35]. Application of this analysis to the gamma alloy [35] indicated that the higher tensile ductility observed in the G1F microstructure was, in reality, a crack size effect, which manifested as a grain size effect. Based on these results, it was concluded that the lamellar microstructure was more fracture-resistant than the equiaxed γ microstructure. Improvement in the tensile ductility of the lamellar microstructure could be achieved by reducing the lamellar colony size to smaller values. The equiaxed gamma grains were considered undesirable and should be minimized or eliminated from the microstructure. Both of these notions were implemented, with successful results, by Metcut-MRG at WPAFB to tailor fully lamellar microstructures for optimized tensile ductility and fracture toughness properties.

The sources of high fracture resistance observed in the lamellar microstructure at 800°C shown in Fig. 24 were not positively identified. The fracture process at 800°C, shown in Fig. 27, was quite similar to that observed at 25°C. In particular, crack extension appeared to occur by crack propagation along the α_2/γ interface and across the lamellae along apparently localized shear bands. Near-tip strain measurements indicated relatively high crack-tip strain values. The near-tip strains in Fig. 28 were, however, lower than those expected based on the Hutchinson [45], Rice, and Rosengren [46] (HRR) field and the remote K values, suggesting the presence of one or more shielding mechanism(s). The high near-tip strain values were consistent with tensile testing performed in vacuum inside the SEM, but were inconsistent with conventional tensile results obtained in air. Comparison of the in-situ tensile test performed in the SEM vacuum with the result obtained in air using the conventional method revealed large discrepancies in the hardening behavior and in the fracture strains. As shown in Fig. 29, the tensile ductility in air was 1.5%, while no fracture was observed after \approx 20% straining in vacuum. In the latter case,

Ti-47Al-2.6Nb-2.0(Cr + V)

800°C

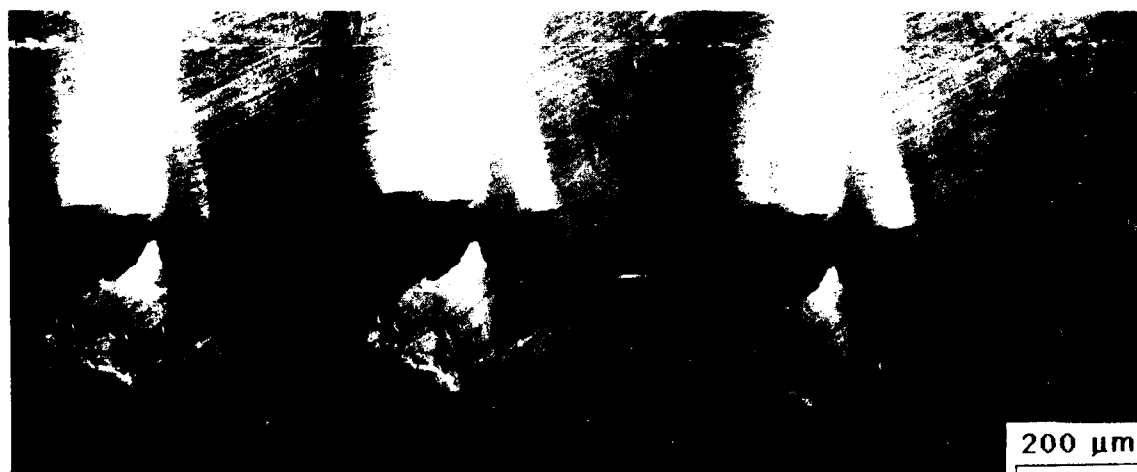
 $K = 36 \text{ MPa}\sqrt{\text{m}}$ $K = 39 \text{ MPa}\sqrt{\text{m}}$ $K = 41 \text{ MPa}\sqrt{\text{m}}$ $K = 48 \text{ MPa}\sqrt{\text{m}}$  $K = 50 \text{ MPa}\sqrt{\text{m}}$ $K = 52 \text{ MPa}\sqrt{\text{m}}$ $K = 57 \text{ MPa}\sqrt{\text{m}}$

Fig. 27 Composite in-situ SEM micrographs showing the near-tip fracture process in the lamellar microstructure at 800°C is characterized by apparent interface growth and translamellar propagation along localized shear bands.

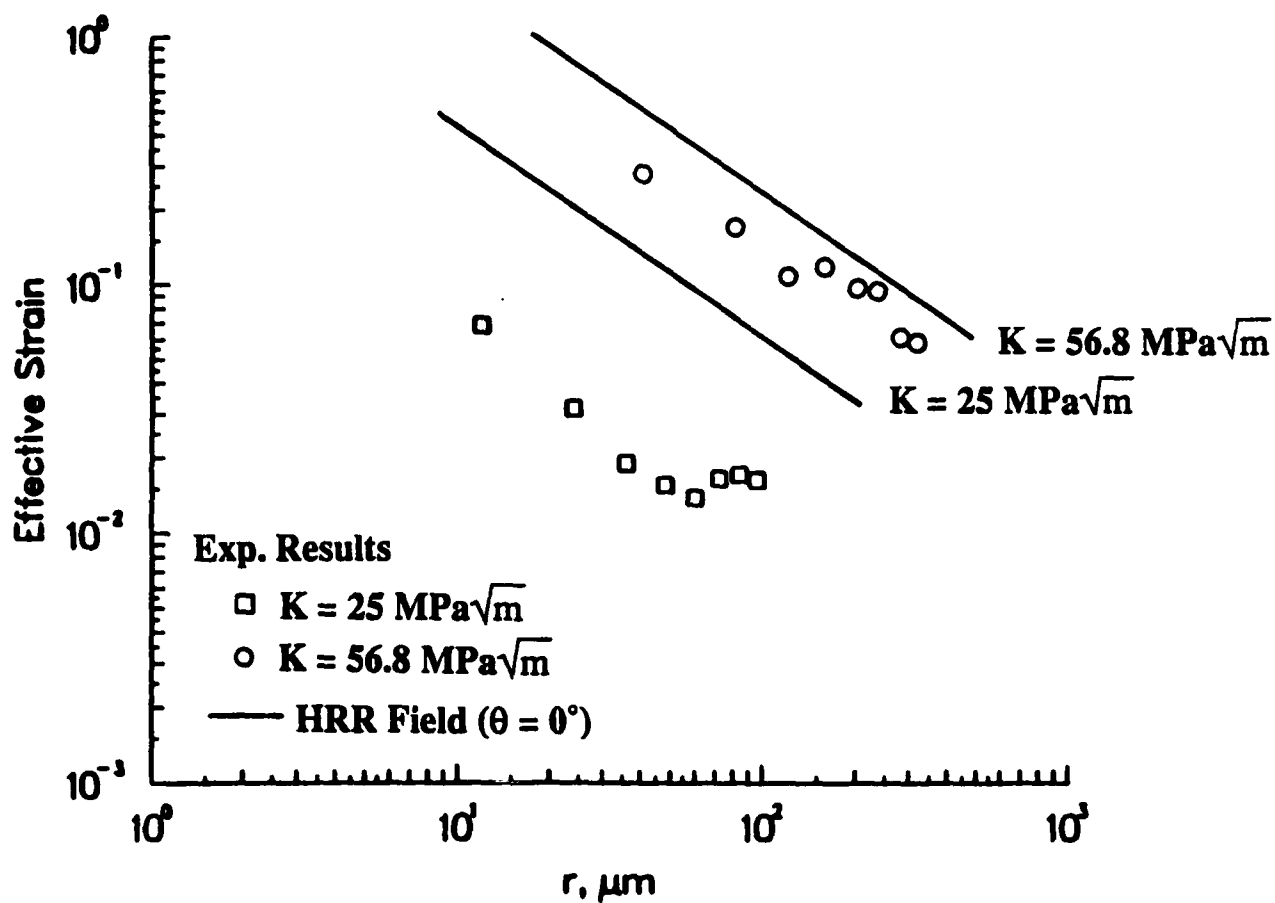


Fig. 28 Comparison of the measured effective strain distributions with the HRR theory at two K levels showing lower measured strain values at a given K level. The discrepancy suggests that the near-tip K values are lower, probably due to the presence of one or more shielding mechanism(s) operative near the crack tip.

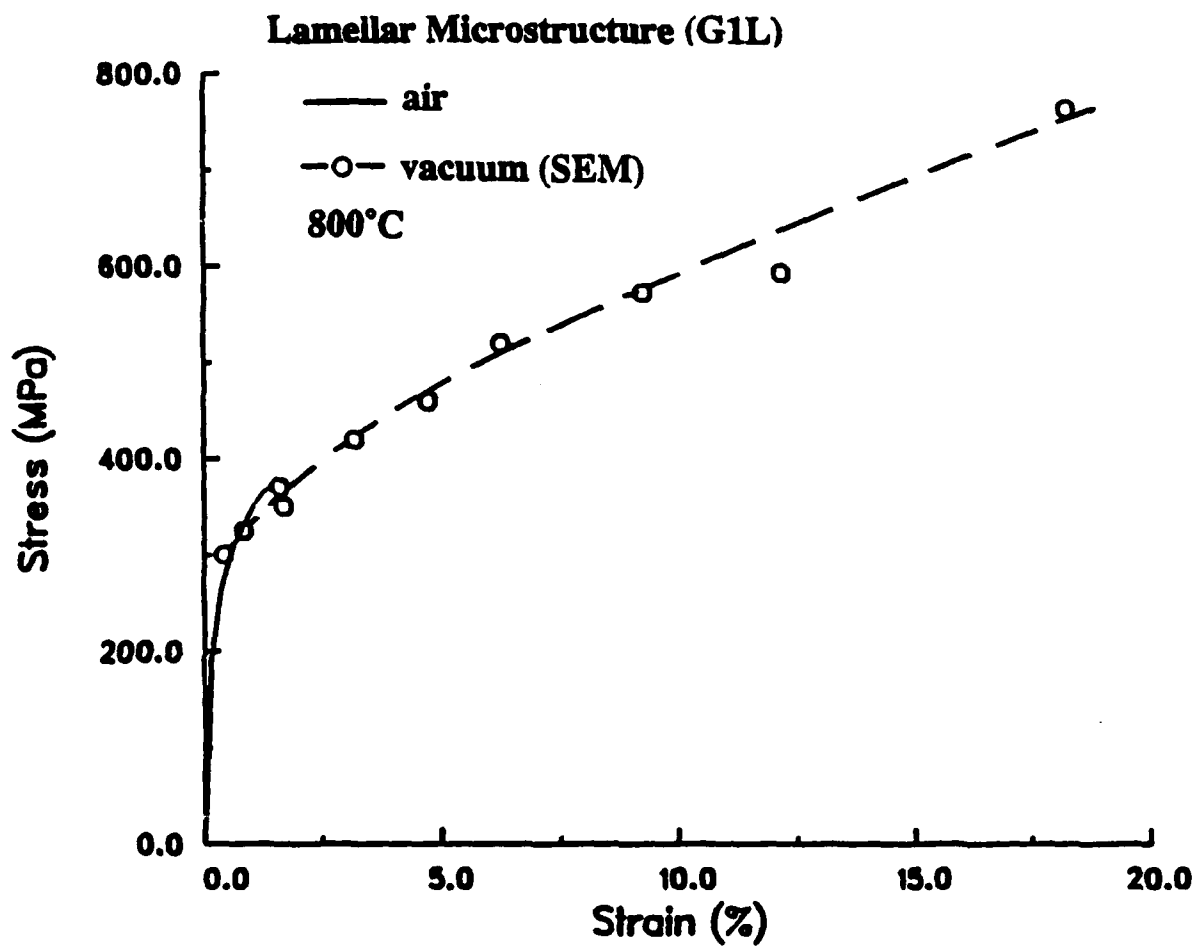


Fig. 29 Comparison of engineering stress-strain curves for the lamellar microstructure tested at 800°C in air and in vacuum.

the higher tensile ductility was found to originate from the ability of the microstructure to prevent microcracks, which were nucleated at boundaries of lamellar colonies, gamma grains, and combinations of those two, from subsequent growth into contiguous lamellar colonies. This set of experimental observations and results suggested the possibility of an environmental embrittlement process in fracture of the lamellar microstructure in air at elevated temperatures. Further work is required to substantiate this hypothesis, however.

C. Overall Assessment of Ductile Phase Toughening in Two-Phase Titanium Aluminide Alloys

Important insights concerning toughness enhancement by a ductile phase in a two-phase microstructure containing a relatively brittle intermetallic matrix were obtained from the studies of toughening mechanisms in the titanium aluminide alloys. From the studies of the Ti-24Al-11Nb alloy, it is apparent that crack-tip blunting by the ductile phase is an important mechanism in imparting initiation toughness. For this mechanism to be effective, a relatively large volume fraction of the continuous ductile phase is preferred over a discontinuous one for the same volume fraction. The ductile phase must also exhibit thermal stability, relatively high strength and toughness at elevated temperatures. The Ti-24-11 result also indicates that the matrix properties cannot be overlooked.

The lamellar microstructure of the near gamma alloy, Ti-47Al-2.6Nb-2(Cr+V), appears to provide many of the attributes which are lacking in the $\alpha_2 + \beta$ microstructure in the Ti-24Al-11Nb alloy. The aligned $\alpha_2 + \gamma$ morphology in the coarse-grained lamellar microstructure provides a naturally continuous ductile phase in the α_2 platelets which the crack tip cannot avoid without a substantial deviation of the crack path from its original mode I direction. The observation that the α_2 is ductile when existed in the form of sub-micron-sized thin plates in the gamma alloy, but is relatively brittle when existed in grain or matrix form in the alpha-two alloy is an amazing result, which indicates that besides alloy composition, the fine microstructural scale in the lamellar microstructure is a desirable and an important feature for imparting toughness in the intermetallic alloy at both ambient and elevated temperatures. Contrasting the overall mechanical properties of Ti-24Al-11Nb against those of Ti-47Al-2.6Nb-2(Cr+V), it becomes apparent that a ductile intermetallic phase is more desirable than a ductile metallic phase as a toughening agent because of its better high-temperature deformation and fracture properties.

V. REFERENCES

1. W. Elber, "Fatigue Crack Closure Under Cyclic Tension," *Eng. Fracture Mech.* **2**, 1970, pp. 37-45
2. **Mechanics of Fatigue Crack Closure**, eds., J. C. Newman and W. Elber, ASTM STP-982, ASTM, Philadelphia, PA, 1988.
3. E. P. Phillips, "Results of the Round Robin on Opening-Load Measurement," NASA Technical Memorandum 101601, Langley Research Center, Hampton, VA, May 1989.
4. A. Ohta, M. Kosuge and E. Sasaki, "Change of Fatigue Closure Level with Gauge Location Along Crack Line," *Int. Journal of Fracture* **15**, R53-R57, 1979.
5. J. W. Jones, D. E. Macha, and D. M. Corbly, "Observations on Fatigue Crack Opening Load Determinations," *Int. Journal of Fracture* **14**, R25-30, 1978.
6. J. L. Horng and M. E. Fine, "Near-Threshold Fatigue Crack Propagation Rates of Dual-Phase Steels," *Materials Sci. and Eng.* **67**, 1984, pp. 185-195
7. R. S. Vecchio, J. S. Crompton, and R. W. Hertzberg, "The Influence of Specimen Geometry on Near Threshold Fatigue Crack Growth," *Fatigue Fract. of Eng. Mat. Struct.* **10**, 1987, pp. 333-342.
8. D. L. Davidson and A. Nagy, "A Low Frequency Cyclic Stage for the SEM," *Journal Physics E* **11**, 1978, pp. 207-210.
9. D. L. Davidson and J. Lankford, "Dynamic, Real-Time Fatigue Crack Propagation at High Resolution as Observed in the Scanning Electron Microscope," in **Fatigue Mechanisms**, ASTM STP-675, ASTM, Philadelphia, PA, 1979, pp. 277-284.
10. S. J. Hudak, Jr. and D. L. Davidson, "The Dependence of Crack Closure on Fatigue Loading Variables," in **Mechanics of Fatigue Crack Closure**, ASTM STP-982, ASTM STP-982, eds., J. C. Newman and W. Elber, ASTM, Philadelphia, PA, 1988, pp. 121-138.
11. D. L. Davidson, "Plasticity Induced Closure," in **Mechanics of Fatigue Crack Closure**, ASTM STP-982, eds., J. C. Newman and W. Elber, ASTM, Philadelphia, PA, 1988, pp. 44-61.

12. D. L. Davidson, "Small and Large Fatigue Cracks in Aluminum Alloys," *Acta Metallurgica* **36**, 1988, pp. 2275-2282.
13. D. L. Davidson and J. Lankford, "The Effect of Aluminum Alloy Microstructure on Fatigue Crack Growth," *Mat. Sci. and Eng.* **74**, 1987, pp. 33-45
14. T. G. F. Gray, "Convenient Closed Form Stress Intensity Factors for Common Crack Configurations," *Int. Journal of Fracture* **13**, 1977, pp. 65-75.
15. D. L. Davidson and J. Lankford, "Mixed Mode Opening in Fatigue," *Mat. Sci. and Eng.* **60**, 1983, pp. 225-229.
16. F. J. Pitoniak, A. F. Grandt, L. T. Montulli, and P. F. Packman, "Fatigue Crack Retardation and Closure in Polymethylmethacrylate," *Eng. Fracture Mech.* **6**, 1974, pp. 547-558.
17. N. A. Fleck, "An Investigation of Fatigue Crack Closure," PhD. Dissertation, Cambridge University, 1984, pp. 191.
18. R. C. McClung and H. Sehitoglu, "On the Finite Element Analysis of Fatigue Crack Closure-1. Basic Modeling Issues," *Eng. Fracture Mech.* **33**, 1989, pp. 237-252.
19. R. C. McClung and D. L. Davidson, "High Resolution Numerical and Experimental Studies of Fatigue Cracks," *Eng. Fracture Mech.* (submitted).
20. B. Budiansky and J. W. Hutchinson, "Analysis of Closure in Fatigue Crack Growth," *J. Appl. Mech.* **45**, 1978, pp. 267-276.
21. H. Tada, P. C. Paris, and G. R. Irwin, "The Stress analysis of Cracks Handbook," Del Research Corp., Hellertown, PA, 1973, pp. 3.4
22. R-H. Zhao, S-H Dai, and J. C. M. Li, "Dynamic Emission of Dislocations from a Crack Tip - A Computer Simulation," *Int. J. Of Fracture* **29**, 1985, pp. 3-20.
23. J. Tirosh and A. Ladelski, "Note on Residual Stresses Induced by Fatigue Cracking," *Eng. Fracture Mech.* **13**, 1980, pp. 453-461.
24. D. Davidson, "The Effect of Particulate SiC on Fatigue Crack Growth in a Cast-Extruded Aluminum Alloy Composite," *Met. Trans. A* **22A**, 1991, pp. 97-112.

25. H. U. Staal and J. D. Elen, "Crack Closure and Influence of Cycle Ratio R on Fatigue Crack Growth in Type 304 Stainless Steel at Room Temperature," *Eng. Fracture Mech.* **11**, 1979, pp. 275-283.
26. M. F. Kanninen and C. H. Popelar, "Advanced Fracture Mechanics," Oxford University Press, New York, 1985, pp. 47.
27. G. R. Yoder, L. A. Cooley, and T. W. Crooker, "A Critical Analysis of Grain-Size and Yield Strength Dependence of Near Threshold Fatigue Crack Growth in Steels," in **Fracture Mechanics, Fourteenth Symposium - Vol. I: Theory and Analysis**, ASTM STP-791, eds., J. C. Lewis and G. Sines, ASTM, Philadelphia, PA, 1983, pp. 348-365.
28. R. O. Ritchie, "Near Threshold Fatigue Crack Propagation in Steels," *Int. Metals Reviews* **20**, 1979, pp. 205-230.
29. D. Taylor, "A Model for the Estimation of Fatigue Threshold Stress Intensities in Materials with Different Microstructures," in **Fatigue Thresholds**, eds., V. I. J. Backlund, A. F. Blom, and C. J. Beevers, EMAS, Cradley Heath, UK, 1982, pp. 455-470.
30. D. L. Davidson, "The Growth of Fatigue Crack Through Particulate SiC Reinforced Aluminum Alloys," *Eng. Fracture Mech.* **33**, 1989, pp. 451-466.
31. S. Suresh, "Crack Initiation in Cyclic Compression and its Application," *Eng. Fracture Mech.* **21**, 1985, pp. 453-463.
32. K. Minikawa and A. J. McEvily, "On Crack Closure in Near Threshold Region," *Scripta Metallurgica* **15**, 1981, pp. 633-636.
33. D. L. Davidson, "Titanium Alloys: Fatigue Crack Growth Mechanisms and Crack Tip Micromechanics," in **Microstructure Property Relationships in Titanium and Titanium Aluminides**, eds., Y.-W. Kim, et al., TMS, Warrendale, PA, 1991 (in press).
34. K. S. Chan, "Influence of Microstructure on Intrinsic and Extrinsic Toughening in an Alpha-Two Titanium Aluminide Alloy," *Metall. Trans. A*, 1991 (submitted).
35. K. S. Chan and Young-Won Kim, "Fracture Processes in a Two-Phase Gamma Titanium Aluminide Alloy," in **Relationships in Titanium Alloys and Titanium Aluminides**, eds., Y.-W. Kim, R. R. Boyer, and J. A. Hall, TMS, Warrendale, PA, 1991 (in press).

36. K. S. Chan, "Theoretical Analysis of Grain Size Effects on Tensile Ductility," *Scripta Metall.*, vol. 24, 1990, pp. 1725-1730.
37. K. S. Chan, "Micromechanics of Shear Ligament Toughening," *Metall. Trans. A*, 1990 (submitted).
38. K. S. Chan, "Fracture and Toughening Mechanisms in the α_2 Titanium Aluminide Alloy," *Metall. Trans. A*, vol. 21A, 1990, pp. 2687-2699.
39. L. R. F. Rose, *Int. J. Fract.*, vol. 31, 1986, pp. 233-242.
40. S. Suresh, *Metall. Trans. A*, vol. 16A, 1985, pp. 249-260.
41. B. Budiansky, J. C. Amazigo, and A. G. Evans, *J. Mech. Phys. Solids*, vol. 36, 1988, pp. 167-88.
42. W. O. Soboyejo, B. A. Abbott, S. Midea, and D. S. Schwartz, unpublished research, McDonald Douglas Research Laboratories, St. Louis, MO (1990).
43. D. P. DeLuca, B. A. Cowles, F. K. Haake, and K. P. Holland, *Fatigue and Fracture of Titanium Aluminides*, WRDC-TR-89, 1989, pp. 4136.
44. R. G. Rowe, J. A. Sutliff, and E. F. Koch, *MRS Symposia Proceedings*, eds., B. G. Girssen, D. E. Polk, and A. I. Taub, vol. 58, MRS, Pittsburgh, PA, 1986, pp. 359-364.
45. J. W. Hutchinson, *J. Mech. Phys. Solids*, vol. 16, 1968, pp. 13-31.
46. J. R. Rice and G. R. Rosengren, *J. Mech. Phys. Solids*, vol. 16, 1968, pp. 1-13.

VI. PUBLICATIONS

1. "Fracture and Toughening Mechanisms in an α_2 Titanium Aluminide Alloy," K. S. Chan, *Metall. Trans. A*, vol. 21A, 1990, pp. 2687-2699.
2. "Application of Scanning Tunneling Microscopy to Fatigue and Fracture," J. Lankford and M. Longmire, *J. of Mater. Sci.*, 1990 (in press).
3. "Theoretical Analysis of Grain Size Effects on Tensile Ductility," K. S. Chan, *Scripta Metall.*, vol. 24, 1990, pp. 1725-1730.
4. "Fracture Processes in a Two-Phase Gamma Titanium Aluminide Alloy," K. S. Chan and Young-Won Kim, in **Microstructure/Property Relationships in Titanium Alloys and Titanium Aluminides**, eds., Y.-W. Kim, R. R. Boyer, and J. A. Hall, TMS, Warrendale, PA, 1991 (in press).
5. "Micromechanics of Shear Ligament Toughening," K. S. Chan, *Metall. Trans. A*, 1990 (submitted).
6. "Influence of Microstructure on Intrinsic and Extrinsic Toughening in an Alpha-Two Titanium Aluminide Alloy," K. S. Chan, *Metall. Trans. A*, 1991 (submitted).
7. "Titanium Alloys: Fatigue Crack Growth Mechanisms and Crack Tip Micromechanics," D. L. Davidson, *ibid* (4).
8. "Fatigue Crack Closure," D. L. Davidson, **Engineering Fracture Mechanics** (accepted 11/90).
9. "Micromechanics of Materials Brittle at Ambient Temperature," D. L. Davidson, in **Micromechanics of Failure of Quasi-Brittle Materials**, eds., S. P. Shah, S. E. Swartz, and M. L. Ming, Elsevier, New York, 1990, pp. 3005-314.
10. "Techniques for Microcrack Mechanics," D. L. Davidson, **ASTM Workshop on Small Crack Test Methods**, eds., J. E. Larsen and J. E. Allison, 1990 (in press).
11. "Fatigue Crack Growth Mechanisms and Mechanics in Metallic and Intermetallic Alloys and Partially Stabilized Zirconia," D. L. Davidson, in **Mechanical Fatigue of Advanced Materials**, eds., R. O. Ritchie, B. N. Cox, and R. Dauskardt, MCEP, 1991 (in press).

VII. PROGRAM PERSONNEL

<u>Name</u>	<u>Title</u>	
Dr. David Davidson	Institute Scientist	} Co-Principal Investigators
Dr. James Lankford	Institute Scientist	
Dr. K. S. Chan	Principal Engineer	
Mr. Harold Saldana	Staff Technician	
Mr. John Campbell	Senior Technician	
Mr. James Spencer	Senior Technician	

VIII. INTERACTIONS

1. TMS Annual Meeting, Anaheim, CA, Feb. 18-22, 1990. K. S. Chan presented a paper entitled "Micromechanics of Static Crack Initiation and Growth in an α_2 Titanium Aluminide Alloy."
2. TMS Fall Meeting, Detroit, MI, Oct. 7-11, 1990. K. S. Chan presented two papers. The first one was entitled "Sources of Fracture Toughness in an α_2 Titanium Aluminide Alloy," while the second paper was entitled "Fracture Processes in a Two-Phase Gamma Titanium Aluminide Alloy." D. L. Davidson presented one paper entitled "Titanium Alloys: Fatigue Crack Growth Mechanisms and Crack Tip Micromechanics."
3. Seminar at University of Michigan, Department of Materials Science, Oct. 29, 1990 by D. L. Davidson - Fatigue in Titanium Aluminides was one of the subjects discussed.
4. Seminar at Rolls-Royce, Inc., Atlanta, GA, Nov. 1, 1990 by D. L. Davidson - Fatigue of Titanium Aluminides was of the subjects discussed.
5. ASTM Workshop on Measurement Techniques for Small Fatigue Cracks, Nov. 14, 1990, San Antonio, TX. "Measurement Techniques for Microcrack Mechanics" by D. L. Davidson included discussions of small crack work in aluminum alloys and titanium aluminides.